Cell Reports

Article

USP32-regulated LAMTOR1 ubiquitination impacts mTORC1 activation and autophagy induction

Graphical abstract

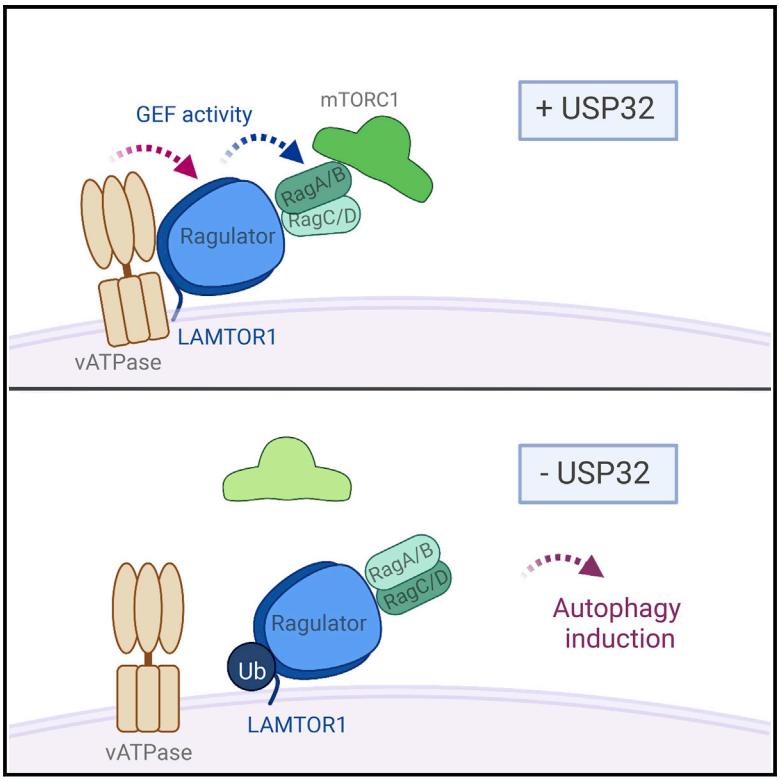

Highlights

- USP32 deubiquitinates the Ragulator complex subunit LAMTOR1 at lysine (K) 20
- LAMTOR1 K20 ubiquitination impairs its binding to the vacuolar H^+-ATPase
- USP32 knockout reduces mTORC1 activity and elevates autophagic flux
- Depletion of USP32 in *Caenorhabditis elegans* inhibits mTOR and induces autophagy

Authors

Alexandra Hertel, Ludovico Martins Alves, Henrik Dutz, ..., Stefan Eimer, Florian Steinberg, Anja Bremm

Correspondence

bremm@em.uni-frankfurt.de

In brief

Hertel et al. identify a control mechanism of the mTORC1 activation cascade at lysosomes via USP32-regulated ubiquitination of LAMTOR1, a Ragulator complex subunit. Increased ubiquitination of LAMTOR1 residue K20 in USP32-deficient cells limits interaction between LAMTOR1 and the vacuolar H^+-ATPase and results in reduced mTORC1 activation and autophagy induction.

Hertel et al., 2022, Cell Reports *41*, 111653
December 6, 2022
https://doi.org/10.1016/j.celrep.2022.111653

CellPress

Cell Reports

CellPress
OPEN ACCESS

Article

USP32-regulated LAMTOR1 ubiquitination impacts mTORC1 activation and autophagy induction

Alexandra Hertel,[1] Ludovico Martins Alves,[2] Henrik Dutz,[3] Georg Tascher,[1] Florian Bonn,[1] Manuel Kaulich,[1,4,5] Ivan Dikic,[1,2,4,5] Stefan Eimer,[6] Florian Steinberg,[3] and Anja Bremm[1,7,*]

[1]Institute of Biochemistry II, Goethe University Frankfurt - Medical Faculty, University Hospital, Theodor-Stern-Kai 7, 60590 Frankfurt am Main, Germany

[2]Buchmann Institute for Molecular Life Sciences, Goethe University Frankfurt, Max-von-Laue-Str. 15, 60438 Frankfurt am Main, Germany

[3]Center for Biological Systems Analysis, University of Freiburg, Habsburgerstr. 49, 79104 Freiburg, Germany

[4]Frankfurt Cancer Institute, 60596 Frankfurt am Main, Germany

[5]Cardio-Pulmonary Institute, 60590 Frankfurt am Main, Germany

[6]Institute of Cell Biology and Neuroscience, Goethe University Frankfurt, Max-von-Laue-Str. 13, 60439 Frankfurt am Main, Germany

[7]Lead contact

*Correspondence: bremm@em.uni-frankfurt.de

https://doi.org/10.1016/j.celrep.2022.111653

SUMMARY

The endosomal-lysosomal system is a series of organelles in the endocytic pathway that executes trafficking and degradation of proteins and lipids and mediates the internalization of nutrients and growth factors to ensure cell survival, growth, and differentiation. Here, we reveal regulatory, non-proteolytic ubiquitin signals in this complex system that are controlled by the enigmatic deubiquitinase USP32. Knockout (KO) of USP32 in primary hTERT-RPE1 cells results among others in hyperubiquitination of the Ragulator complex subunit LAMTOR1. Accumulation of LAMTOR1 ubiquitination impairs its interaction with the vacuolar H^+-ATPase, reduces Ragulator function, and ultimately limits mTORC1 recruitment. Consistently, in USP32 KO cells, less mTOR kinase localizes to lysosomes, mTORC1 activity is decreased, and autophagy is induced. Furthermore, we demonstrate that depletion of USP32 homolog CYK-3 in *Caenorhabditis elegans* results in mTOR inhibition and autophagy induction. In summary, we identify a control mechanism of the mTORC1 activation cascade at lysosomes via USP32-regulated LAMTOR1 ubiquitination.

INTRODUCTION

Ubiquitination is a reversible post-translational modification (PTM) that regulates most cellular processes. Tens of thousands of unique ubiquitination sites in the human proteome were identified by mass spectrometry-based approaches,[2] supporting the widespread involvement of the highly dynamic and complex ubiquitin system in cell functions. Ubiquitin molecules are attached to substrate proteins by the sequential activities of E1 (ubiquitin-activating), E2 (ubiquitin-conjugating), and E3 (ubiquitin ligase) enzymes. In contrast, deubiquitinating enzymes (DUBs) cleave ubiquitin from substrate proteins, edit ubiquitin chains, and process ubiquitin precursors. Thus, DUBs are key to a precise cellular outcome of ubiquitin signals.[3] Deregulation of DUBs has been observed in a variety of sporadic and genetic disorders like cancer, neurodegeneration, and inflammatory diseases. Consequently, great efforts are directed in the development of specific DUB inhibitors for clinical use.[4,5]

The human genome encodes ~100 DUBs that are classified in seven families based on sequence and domain conservation.[6] Although the physiological function of various DUBs and their roles in disease has, at least in part, been uncovered, we are still lacking this knowledge for numerous other DUBs. Among this group is the ubiquitin-specific protease (USP) 32, a unique and highly conserved member of the USP family DUBs. USP32 is a multi-domain protein that comprises the catalytic USP domain, a DUSP domain that is predicted to mediate protein-protein interactions, two ubiquitin-like (UBL) domains, as well as N-terminal calcium-binding EF hands, and a C-terminal prenylation site (CAAX box), both of which are unique among all human DUBs.

Already a decade ago, USP32 has been described as active, membrane-bound ubiquitin protease that is overexpressed in breast cancer.[7] Meanwhile, additional reports proposed an oncogenic role for USP32 in small cell lung cancer,[8] gastric cancer,[9] and epithelial ovarian cancer.[10] Silencing of USP32 reduced cancer cell proliferation and migration in these studies and suggested USP32 as potential target for future therapy, although the tumor-promoting effects of USP32 are not fully understood yet. Recently, USP32 also emerged as regulator of late endosomal transport and recycling, it was shown to deubiquitinate Rab7.[11]

The endosomal-lysosomal system is a highly organized network in eukaryotic cells comprising a series of dynamic membrane-enclosed organelles and vesicles, like early endosomes (EE), recycling endosomes (RE), late endosomes (LE), and lysosomes.[12] The endosomal-lysosomal system executes trafficking

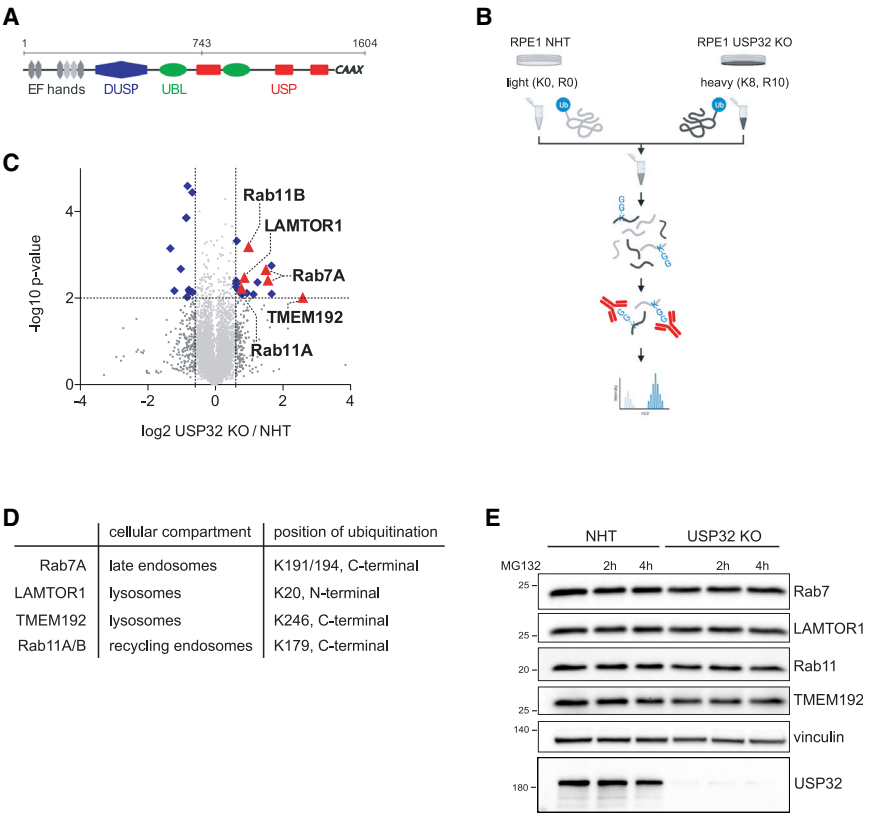

Figure 1. USP32 substrate identification

(A) Schematic overview of the predicted domain architecture of USP32.

(B) Experimental setup of SILAC-based quantitative ubiquitin-modified proteome analysis in RPE1 cells to determine potential USP32 substrates.

(C) Volcano plot depicting identified diGly remnant peptides in USP32 KO (heavy) over control NHT (light) cells (n = 3). Identified peptides with fold change log2 ratio $\geq$0.6 or $\leq$ −0.6 and -log10 p value $\geq$ 2 were considered as significantly enriched or depleted, respectively (labeled in blue). Significantly enriched proteins of the endosomal-lysosomal system interesting for further validation are labeled in red.

(D) Table showing selected USP32 substrates, their main cellular localization, and the identified regulated diGly site(s) in USP32 KO cells.

(E) USP32 cleaves non-proteolytic signals from endosomal-lysosomal proteins. RPE1 NHT and USP32 KO cells were either untreated or treated for 2 h and 4 h with 10 μM MG132, and protein levels were detected by western blotting. See also Figure S1.

and degradation of proteins and lipids, and mediates the internalization of nutrients and growth factors to ensure cell survival, growth, and differentiation. The small GTPase Rab7 coordinates most steps during maturation of EE to LE and lysosomes. Rab7 is enriched at LE where it cycles between a cytosolic and a membrane-attached state closely linked to its nucleotide status.[13] In addition, Rab7 function can be modulated by several PTMs like phosphorylation, lipidation, and ubiquitination, which can facilitate or prevent interaction with specific effector proteins.[14]

Besides its role in protein degradation and recycling, lysosomes are dynamic signaling hubs that sense the nutrition status of the cell and control the switch between anabolism and catabolism by regulating lysosomal biogenesis and autophagy.[15] A major receiver of lysosomal signals is the mechanistic target of rapamycin (mTOR) complex 1 (mTORC1). Kinase activity of this complex is regulated by a multistep process involving a network of interacting proteins.[16] In response to amino acid stimulation, mTORC1 is recruited to lysosomes by heterodimeric Rag small GTPases, which are themselves tethered to the lysosome by the pentameric Ragulator protein complex.[17] Together with arginine-primed amino acid transporter (SCL38A9), Ragulator acts as guanine nucleotide exchange factor (GEF) for the Rag heterodimers.[18–21] It was suggested that interaction with the vacuolar H^+-ATPase (v-ATPase) triggers in turn full activity of the Ragulator/SLC38A GEF complex. Ultimately, after its recruitment to the lysosome, mTORC1 is activated by the small GTPase Rheb.

Activity of mTORC1 is further regulated by ubiquitin-mediated proteasomal degradation of mTORC1 signaling pathway components, e.g., TSC1/2, Rheb or subunits of the Ragulator complex.[22–24] Knowledge about non-proteolytic ubiquitin signals in this context and their function in the dynamic modulation of protein activity, interaction, or localization is only emerging and detailed molecular mechanisms remain to be determined.

In this study, we aimed to characterize the cellular function of the deubiquitinase USP32. We identified USP32-regulated, non-proteolytic ubiquitin signals on components of the endosomal-lysosomal system, among them Rab7 and the Ragulator subunit LAMTOR1. Our data showed that USP32 controls Ragulator function by deubiquitinating LAMTOR1 at lysine residue 20 (K20), thereby promoting the interaction between the lysosomal v-ATPase and LAMTOR1. In the absence of USP32, non-proteolytic LAMTOR1 ubiquitination accumulates, which prevents its efficient interaction with v-ATPase and results in decreased mTORC1 recruitment and activation, and increased autophagy induction. In summary, we described USP32-regulated LAMTOR1 ubiquitination as an additional control layer of the mTORC1 activation cascade at lysosomes.

RESULTS

USP32 knockout enriches ubiquitinated proteins of the endosomal-lysosomal system

The deubiquitinase (DUB) USP32 belongs to the ubiquitin-specific proteases. USP32 is the only human DUB that contains a C-terminal prenylation site (CAAX box), which suggests that it can be incorporated into membranes (Figure 1A). Subcellular fractionation experiments using different cell lines showed that endogenous USP32 was indeed present in both the cytoplasmic and the membrane fraction (Figure S1A). GFP-tagged USP32

CellPress
OPEN ACCESS

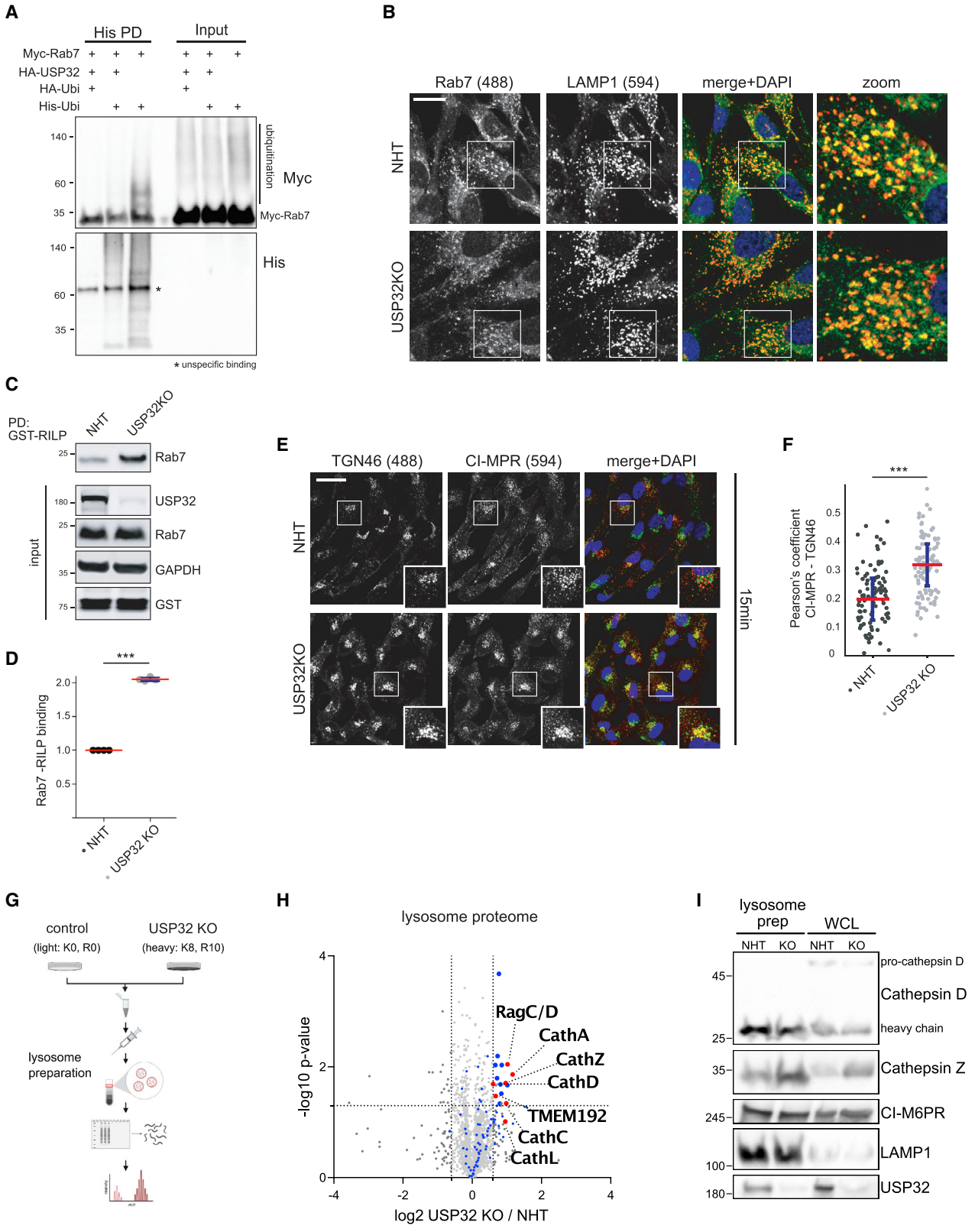

(legend on next page)

localizes to the *trans*-Golgi network.[7] Our immunofluorescence microscopy analysis confirmed colocalization of endogenous USP32 and the Golgi marker GM130 (Figure S1B). USP32 expression has been correlated with tumorigenesis,[7–9] but the physiological function of the enzyme was unknown when we started our investigations. In order to identify the specific cellular processes in which USP32 is involved and to understand how USP32 may regulate them, we aimed to characterize USP32 substrates in human telomerase reverse transcriptase (hTERT) immortalized primary RPE1 cells. We performed a stable isotope labeling with amino acids in cell culture (SILAC)-based, quantitative ubiquitin-modified proteome analysis (diGly remnant profiling) comparing control non-human targeting (NHT) and USP32 knockout (KO) cells (Figure 1B). Interestingly, we observed an accumulation of several ubiquitinated proteins associated with the endosome-lysosome system in USP32 KO cells, for example the small GTPases Rab7 and Rab11, the lysosomal transmembrane protein TMEM192, and the Ragulator component LAMTOR1 (Figures 1C and 1D), all of which coincide with the cellular localization of USP32. Expression levels of the potential USP32 substrates were comparable in control and USP32 KO cells, both in untreated cells and upon proteasome inhibition (Figure 1E), suggesting that USP32 does not regulate proteasomal degradation of these proteins but rather counteracts non-proteolytic ubiquitin signals.

USP32 regulates Rab7 ubiquitination and function

First, we investigated the cellular function of USP32-sensitive Rab7 ubiquitination. Our data indicated that USP32 mainly cleaves ubiquitin from lysine (K) residues 191 and 194 (Figure 1D). Rab7 is a key regulator of membrane trafficking at LEs.[25] To confirm that Rab7 is deubiquitinated by USP32, Rab7 ubiquitination was monitored in the presence and absence of exogenous USP32. His-tagged ubiquitin was expressed together with Myc-Rab7 and HA-USP32 or an empty vector control in HEK 293 cells. His-ubiquitin pulldown experiments and subsequent detection of Myc-Rab7 by immunoblot analysis revealed increased ubiquitination of Rab7, visible as smear that resulted from slower migrating modified Myc-Rab7 species, when USP32 was not co-expressed (Figure 2A). A comprehensive analysis of the ubiquitinated proteome identified multiple ubiquitination sites in Rab7.[2] The E3 ubiquitin ligase Parkin ubiquitinates Rab7 preferentially at K38. This modification is required for efficient translocation of Rab7 to membranes.[26] To test if modulation of Rab7 ubiquitination at K191/194 by USP32 also affects Rab7 positioning, we investigated colocalization of the small GTPase and the lysosomal protein LAMP1 in RPE1 control and USP32 KO cells. Immunofluorescence microscopy analysis showed no significant differences in Rab7 localization relative to LAMP1-positive structures in these cell lines (Figure 2B).

Active, GTP-bound Rab7 associates with various effectors to orchestrate its diverse functions, such as lysosomal biogenesis, late endosome-lysosome fusion, autophagosome maturation, and cargo transport, within the late endocytic network.[25] Activity of Rab7 can be monitored by an effector pulldown assay based on the affinity of active, GTP-loaded Rab7 for its lysosomal effector RILP.[27] Interestingly, Parkin-mediated ubiquitination of Rab7 at K38 promotes its binding to RILP.[26] Therefore, we analyzed how loss of USP32 affects the Rab7-RILP interaction. We observed that more Rab7 bound to the GST-RILP probe in lysates from USP32 KO cells as compared with control cells (Figures 2C and 2D). This observation suggested that Rab7 is either more active or has a higher affinity for the effector protein RILP in RPE1 cells depleted of USP32.

Since our data implicated that Rab7 binding to effector proteins is regulated by USP32, we compared cellular functions of Rab7 in control and USP32 KO cells. A global proteomic analysis of DUBs and their associated protein complexes suggested an interaction between USP32 and the retromer complex.[28] The retromer complex functions as regulator of endocytic recycling that transports a vast variety of transmembrane proteins from endosomes back to the cell surface and also the *trans*-Golgi network (TGN).[29] Based on the cellular localization of USP32 and the suggested interaction with VPS35, a component of the mammalian retromer's cargo-selective trimer (CRC, consisting of VPS35, VPS26, and VPS29), we hypothesized that USP32 could play a role in retromer function. We observed that CRISPR-Cas9-mediated USP32 knockout in RPE1 or U2OS cells did not alter expression levels of retromer components (Figure S2A). Furthermore, co-immunoprecipitation (co-IP) of VPS35 with VPS26 and VPS29 showed no difference in the composition of the cargo-selective trimer upon USP32 KO (Figure S2B). Therefore, we

Figure 2. USP32-sensitive ubiquitination regulates Rab7 function

(A) Overexpression of USP32 decreases Rab7 ubiquitination. His-tagged ubiquitin pulldown assay performed in 293 cells co-expressing His-ubiquitin and Myc-Rab7 in the absence or presence of HA-USP32.

(B) Endogenous Rab7 does not change its localization relative to LAMP1 stained lysosomes in USP32-deficient RPE1 cells. RPE1 NHT and USP32 KO cells were stained for Rab7 and LAMP1. Scale bar, 20 μm.

(C) RILP pulldown assay showing increased Rab7-RILP binding in USP32 KO cells. Recombinant GST-RILP bound to glutathione agarose beads was incubated with lysates from RPE1 NHT and USP32 KO cells to precipitate binding partners. Co-precipitated Rab7 was detected by western blotting.

(D) Quantification of Rab7 bound to GST-RILP beads normalized to Rab7 input levels shown as mean ± SD (***p value < 0.001, unpaired Student's t test; n = 4).

(E) Rab7-mediated retrograde trafficking is enhanced in the absence of USP32. RPE1 NHT and USP32 KO cells were incubated with an antibody against the extracellular (luminal) domain of endogenous CI-MPR for 15 min at 37°C, followed by fixation and staining for the internalized antibody and TGN marker TGN46. Scale bar, 15 μm.

(F) Colocalization as shown by Pearson's coefficient was assessed across 10 images from two independent experiments (***p value < 0.001, unpaired Student's t test).

(G) Experimental setup of SILAC-based quantitative lysosomal proteome analysis in U2OS cells.

(H) Volcano plot depicting identified peptides in USP32 KO (heavy) over control NHT (light) cells (n = 3). Peptides with fold change log2 ratios ≥ 0.6 or ≤ -0.6 and $-$log10 p value ≥ 1.3 were considered as significantly enriched or depleted, respectively. Detected lysosomal proteins are labeled in blue, lysosomal enzymes of interest are labeled in red.

(I) Western blot analysis of whole cell lysates and lysosome fractions isolated from NHT and USP32 KO cells. See also Figure S2.

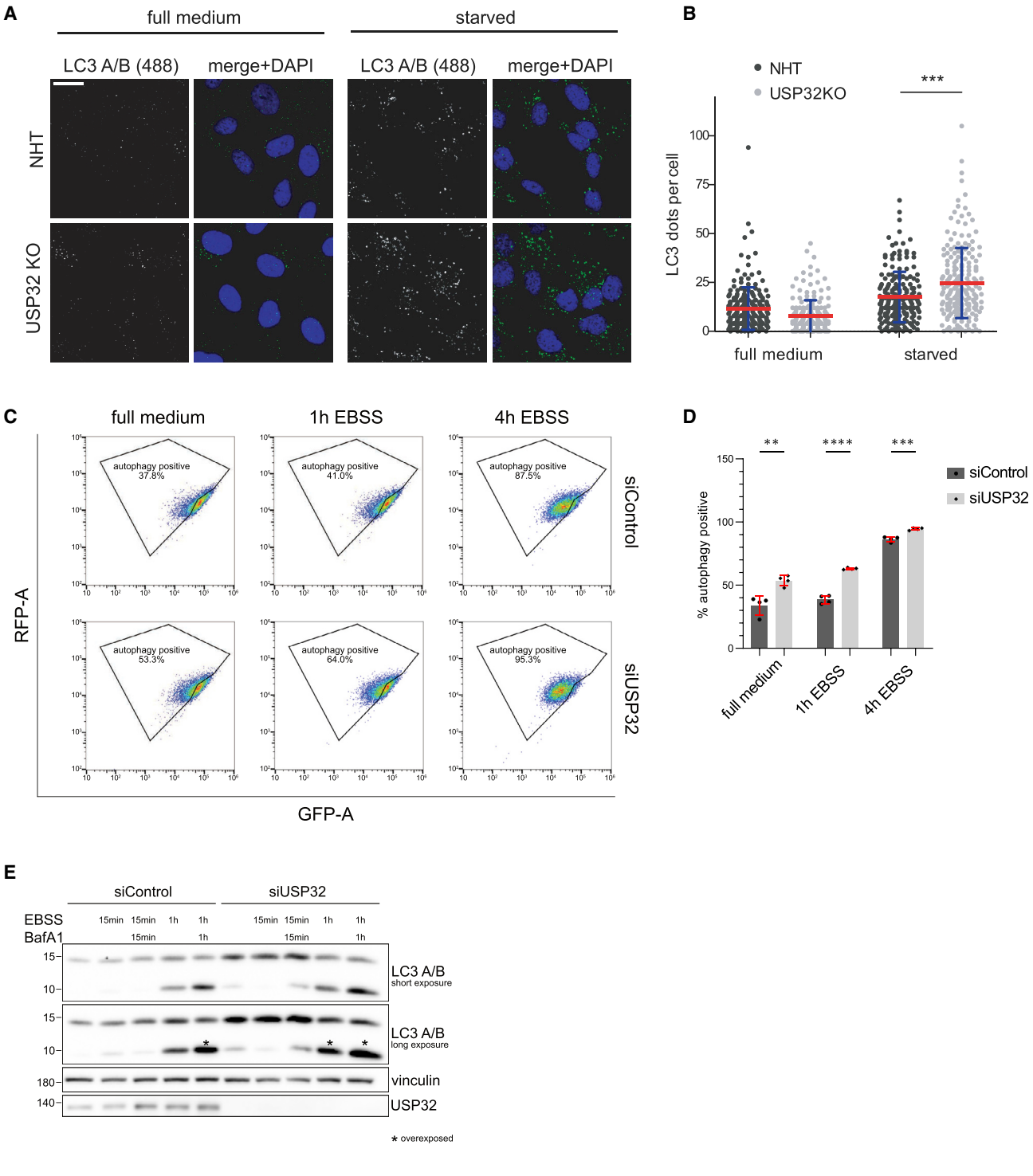

Figure 3. Loss of USP32 induces autophagy

(A) Representative immunofluorescence microscopy images of LC3A/B staining in control and 2 h amino acid-starved RPE1 NHT and USP32 KO cells. Scale bar, 20 μm.

(B) Quantification of LC3-positive dots shown as number of dots per cell with indicated mean ± SD, ***p value < 0.001, unpaired Student's t test (n = 2).

(legend continued on next page)

concluded that USP32 neither influences expression level nor assembly of the CRC and we further investigated retromer-mediated receptor trafficking.

Lysosomal enzymes are diverted from the biosynthetic secretory pathway to the endocytic pathway at the TGN and then progress to highly acidic lysosomes. The best understood route requires phosphorylation of mannose residues in the Golgi apparatus and subsequent shuttling to endosomes, as cargo bound to the cation-independent (CI-MPR) or cation-dependent (CD-MPR) mannose 6-phosphate receptor. Retrieval of receptors from endosomes back to the TGN is mediated by the retromer complex.[29]

By monitoring CI-MPR, the best-characterized cargo for mammalian retromer, we observed that in USP32 KO cells, retrograde transport was accelerated. Our data showed that 15 min after uptake of an antibody against the extracellular domain of CI-MPR, more internalized antibody co-localized with the TGN marker TGN46 (Figures 2E and 2F). In addition, staining of endogenous CI-MPR and the TGN marker Giantin revealed that CI-MPR localization at the TGN was increased in USP32 KO cells (Figures S2C and S2D).

To investigate if altered CI-MPR retrieval in USP32-deficient cells affects sorting of lysosomal hydrolases, we isolated lysosomes by density gradient centrifugation from SILAC-labeled control and USP32 KO U2OS cells and determined the proteome of the organelles by mass spectrometry (Figure 2G). Among others, we observed an enrichment of multiple cathepsins in lysosomes derived from USP32 KO cells as compared with lysosomes isolated from control cells (Figure 2H). In addition to altered sorting, cathepsin Z expression level seemed to be upregulated in USP32 KO cells (Figure 2I).

Loss of USP32 induces autophagy

Meanwhile, Ovaa and colleagues published a study linking USP32 to LE trafficking and recycling.[11] Their data also showed that USP32 deubiquitinates Rab7, which impacts binding efficiency of the small GTPase to different effector proteins and thereby regulates Rab7 function. To distinguish our work from this study, and given that Rab7 is important for autophagosome and autolysosome maturation,[30] we shifted our focus and further investigated the consequences of hyperubiquitination of Rab7 in USP32-deficient cells on autophagy. We quantified LC3-positive autophagosomes by immunofluorescence microscopy. Upon amino acid starvation (EBSS medium), the number of autophagosomes was increased in USP32 KO cells (Figures 3A, 3B, S3A, and S3B). In addition, we monitored autophagic flux using two complementary methods[31] and chose a small interfering RNA (siRNA) pool for USP32 knockdown consisting of 30 optimally designed siRNAs that were demonstrated to efficiently remove off-target effects.[32] First, we generated U2OS cells stably expressing the autophagy flux probe GFP-LC3-RFP-LC3ΔG.[33] This probe is cleaved by endogenous ATG4 proteases into equimolar amounts of GFP-LC3 and RFP-LC3ΔG. GFP-LC3 is degraded by autophagy, whereas conjugation-deficient RFP-LC3ΔG remains in the cytosol and serves as an internal control. We monitored GFP and RFP fluorescent signals in control and USP32 knockdown cells by flow cytometry and calculated the GFP-RFP signal ratio (Figures 3C and 3D). Loss of USP32 significantly increased autophagic flux. Second, lipidation of the autophagy marker LC3 (LC3-II) was analyzed. Stronger accumulation of LC3-II in USP32 knockdown cells briefly treated with EBSS and the vacuolar H^+-ATPase inhibitor Bafilomycin A1, which prevents fusion between autophagosomes and lysosomes as well as lysosomal degradation, suggested elevated autophagy induction in these cells (Figure 3E).

Taken together, our data indicated that Rab7 function can be modulated by USP32-sensitive ubiquitination and that USP32 deficiency resulted in altered retromer-mediated trafficking and autophagy induction.

USP32 deubiquitinates LAMTOR1 and impacts Ragulator function

The latter observation was especially intriguing because our ubiquitin-modified proteome analysis revealed that the Ragulator complex component LAMTOR1 is ubiquitinated within its N-terminal region at lysine residue (K) 20, and that this modification is increased in USP32 KO cells (Figures 1C and 1D), establishing LAMTOR1 as a potential USP32 substrate. The lysosomal Ragulator complex is best known as an essential activation platform for metabolic signaling.[15] LAMTOR1 is one of five subunits forming the Ragulator complex and it anchors the complex to lysosomal membranes via its N-terminal myristoyl and palmitoyl groups at amino acids G2 and C3/C4, respectively. Ragulator is involved in the regulation of mTOR complex 1 (mTORC1) activity and thereby autophagy induction. Given our observation that USP32 KO alters autophagic flux, and that USP32 regulates an ubiquitination event close to the N-terminus of LAMTOR1, a region that is essential for Ragulator positioning to lysosomes and activation of mTORC1,[34,35] it may be possible that USP32 impacts autophagy both by deubiquitinating Rab7 and the Ragulator complex, thereby ultimately modulating mTORC1 activity.

To prove our hypothesis, we first confirmed USP32-sensitive LAMTOR1 ubiquitination using label-free mass spectrometry. LAMTOR1-GFP was immunoprecipitated from control and USP32 KO RPE1 cells. Ubiquitination sites were determined by liquid chromatography-tandem mass spectrometry (LC-MS/MS) analysis and revealed LAMTOR1 modification at K20, K31, K60, and K104 (Figures 4A, 4B and S4A). However, only ubiquitination at K20 was significantly enriched in the absence of USP32.

(C) Representative scatterplots showing negative control (siControl) and USP32 knockdown (siUSP32) U2OS cell populations expressing the GFP-LC3-RFP-LC3ΔG autophagy flux probe. USP32 knockdown decreased GFP/RFP ratios under basal conditions as well as upon amino acid starvation (1 h and 4 h EBSS treatment), indicative of higher autophagic flux.

(D) Quantification of autophagy-positive cells based on gates shown in (C) revealed a significant increase in autophagy in USP32 knockdown cells as compared with control cells (shown as mean ± SD, **p value < 0.01, ***p value < 0.001, ****p value < 0.0001, unpaired Student's t test, n = 4).

(E) RPE1 cells were transfected with siPOOLs: either non-targeting control siRNAs or siRNAs targeting USP32. After amino acid starvation (EBSS) and/or treatment with 200 nM Bafilomycin A1 for the indicated time points, LC3A/B levels were detected by western blotting. See also Figure S3.

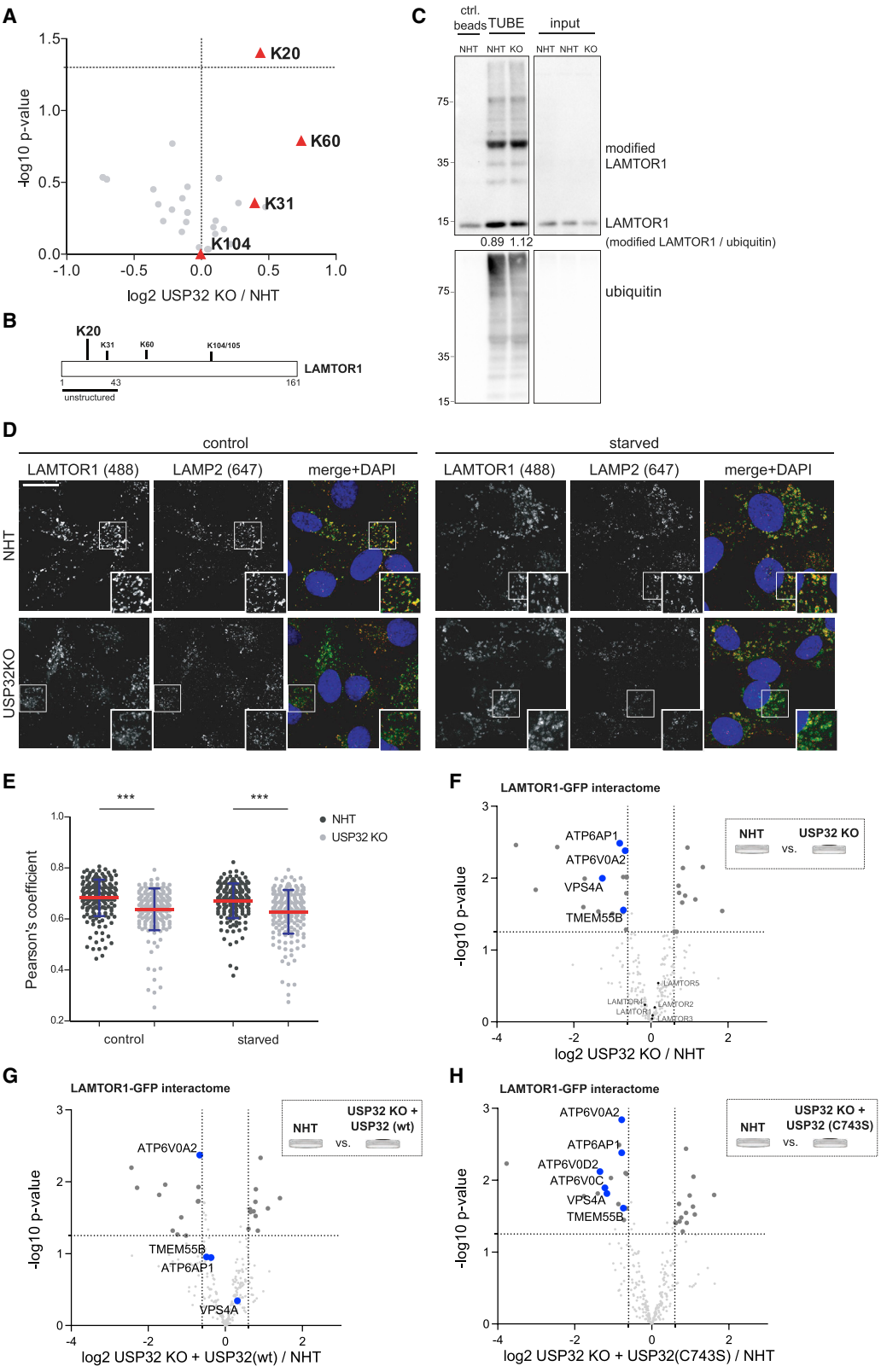

(legend on next page)

In parallel, we used tandem ubiquitin binding entities (TUBEs)[36] to isolate polyubiquitinated proteins from lysates of control and USP32 KO cells and observed enrichment of modified LAMTOR1 in the TUBE-pulldown sample derived from USP32-deficient cells as compared with control cells (also shown as relative density of modified LAMTOR1 signal normalized to ubiquitin signal) (Figure 4C). In addition, His-ubiquitin pulldown experiments were performed to further verify USP32-regulated LAMTOR1 ubiquitination. His-tagged ubiquitin was co-expressed with wild-type (WT) or mutant LAMTOR1-GFP and HA-USP32 in HEK293 cells and subsequently precipitated using Ni-NTA beads. LAMTOR1 modification was detected as high molecular weight smear on a western blot (Figure S4B). Co-expression of catalytic inactive USP32 (C743S) moderately increased LAMTOR1 ubiquitination as compared with WT USP32.

Recently, the E3 ubiquitin ligase UBE3A has been shown to target LAMTOR1 for proteasomal degradation by mainly modifying K60 and K103/K104.[34] However, abundance of LAMTOR1 was not affected in USP32 KO cells (Figure 1E), suggesting that enriched USP32-sensitive ubiquitination of LAMTOR1 at K20 does not promote its proteasomal degradation. Rather, we hypothesized that a ubiquitin molecule or polymer conjugated to K20, i.e., in relatively close proximity to the N-terminus, may interfere with LAMTOR1 localization to lysosomes and hence Ragulator function and ultimately mTORC1 activation. LAMTOR1 and the lysosomal marker LAMP2 were co-stained in both RPE1 and U2OS control and USP32 KO cells under basal or amino acid-starved conditions. In the absence of USP32, LAMTOR1 localization to LAMP2-positive structures was decreased (Figures 4D, 4E, S4C, and S4D), suggesting that deubiquitination by USP32 is required for efficient LAMTOR1 positioning to the lysosome in an amino acid-independent manner.

Full activation of mTORC1 at the lysosomal surface in response to amino acid availability requires the interaction and activity of multiple proteins. The lysosomal v-ATPase senses amino acid levels and stimulates the GEF activity of Ragulator, which scaffolds heterodimeric Rag GTPases and activates them.[21] Activated Rags have increased affinity toward mTORC1 and recruit the kinase complex to the lysosomal surface, the site of its activation by GTP-binding protein Rheb. To examine if K20-ubiquitination of LAMTOR1 impacts the interaction with other Ragulator components or other proteins at the lysosomal surface, we used label-free mass spectrometry to determine the interactome of LAMTOR1-GFP in control and USP32 KO RPE1 cells (Figure 4F). Binding of LAMTOR2-5 to LAMTOR1-GFP was equal in both cell lines, suggesting that increased ubiquitination of LAMTOR1 does not alter the interaction with the other Ragulator subunits und hence complex formation. However, we detected reduced binding between LAMTOR1 and subunits of the lysosomal v-ATPase. This observation was also confirmed by LAMTOR1-GFP immunoprecipitation and subsequent western blot analysis of co-precipitated, endogenous v-ATPase subunits (Figure S4E). Interestingly, this phenotype could be rescued by expression of exogenous, WT HA-USP32 in USP32-depleted cells (Figure 4G) but not by expression of catalytic inactive HA-USP32 (C743S) (Figure 4H). In the presence of inactive USP32 (C743S) binding of LAMTOR1 to multiple v-ATPase subunits was significantly reduced, which suggests that USP32 needs to deubiquitinate LAMTOR1 for its efficient interaction with the lysosomal v-ATPase.

LAMTOR1 ubiquitination reduces mTORC1 recruitment and activation

Since association of v-ATPase with Ragulator under nutrient-rich conditions is a prerequisite for activation of Rag GTPases and mTORC1 recruitment and activation, we investigated if enriched LAMTOR1 ubiquitination in USP32 KO cells impacts localization and activity of mTORC1. Using immunofluorescence microscopy, we analyzed colocalization of the serine/threonine-protein kinase mTOR, which is part of the mTORC1 complex, and the lysosomal protein LAMP2 in control and USP32 KO cells (Figure 5A). Indeed, in the absence of USP32, the localization of mTOR relative to LAMP2 was decreased both under basal and amino acid-starved conditions as shown by the Pearson's correlation coefficient (Figure 5B).

Reduced mTORC1 at the lysosomal membrane results in impaired activation of the kinase complex and reduced phosphorylation of target proteins. We investigated if altered mTOR localization in USP32 KO cells also translates in decreased mTORC1 activity. Therefore, we starved NHT control and USP32 KO RPE1 cells for 16 h and released the cells in full medium for the indicated times. Reactivation of mTORC1 in full medium within 1 h was observed by phosphorylation of downstream substrates pULK1 (S757), pWIPI2 (S413), and pAMBRA1

Figure 4. LAMTOR1 ubiquitination regulates its interaction with v-ATPase

(A) USP32 KO enriches LAMTOR1 ubiquitination at lysine residue 20 (K20). LAMTOR1-GFP was immunoprecipitated from RPE1 NHT and USP32 KO cells and analyzed by LC-MS/MS. Volcano plot showing identified ubiquitination sites (diglycyl lysine residues) of LAMTOR1 in USP32 KO over NHT control cells (n = 3).

(B) Schematic overview of USP32-sensitive ubiquitination site in LAMTOR1.

(C) Tandem ubiquitin binding entities (TUBEs) pulldown assay. Ubiquitinated proteins were enriched from control and USP32 KO cells using TUBEs conjugated to magnetic beads. Ubiquitinated LAMTOR1 was detected using a LAMTOR1-specific antibody.

(D) Lysosomal localization of LAMTOR1 is reduced in USP32 KO cells. Representative immunofluorescence microscopy images of LAMTOR1 and LAMP2 co-staining in untreated and 2 h amino acid-starved RPE1 NHT and USP32 KO. Scale bar, 20 μm.

(E) Quantification of LAMTOR1 colocalization to LAMP2 positive structures shown as Pearson's colocalization coefficient (per cell) with indicated mean ± SD, ***$p < 0.0001$, unpaired Student's t test (n = 3).

(F–H) Label-free mass spectrometry LAMTOR1-GFP interactome study. LAMTOR1-GFP was immunoprecipitated from RPE1 NHT and USP32 KO cells (F) or USP32 KO cells expressing either wild-type HA-USP32 (G) or catalytic inactive HA-USP32(C743S) (H) and interaction partners were analyzed by LC-MS/MS. Volcano plots depicting identified peptides in USP32 KO over control NHT cells (n = 3). Peptides with fold change log2 ratios ≥ 0.6 or ≤ -0.6 and $-\log10$ p value ≥ 1.3 were considered as significantly enriched or depleted, respectively (labeled in dark gray). Subunits of lysosomal v-ATPase and other proteins of interest are labeled in blue. See also Figure S4.

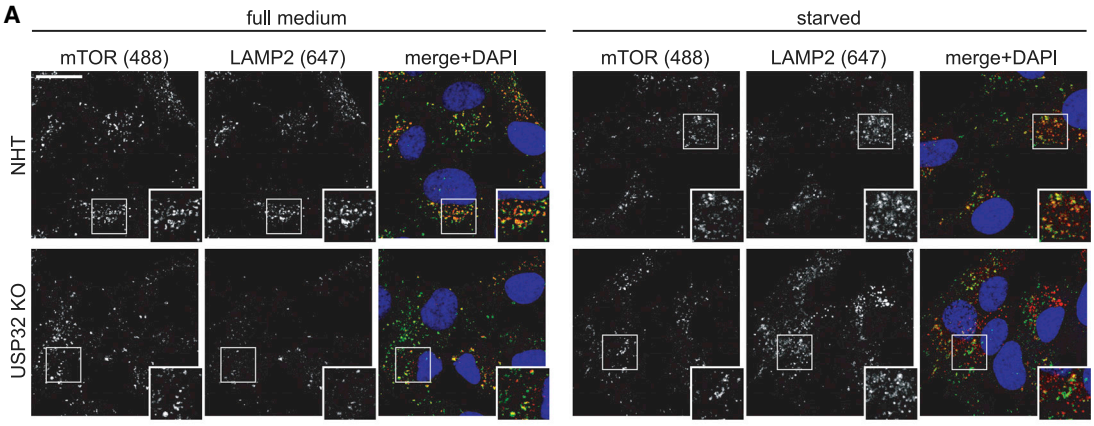

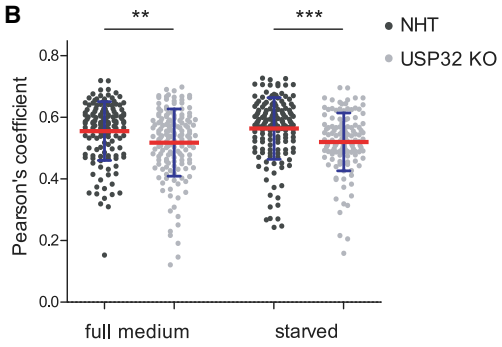

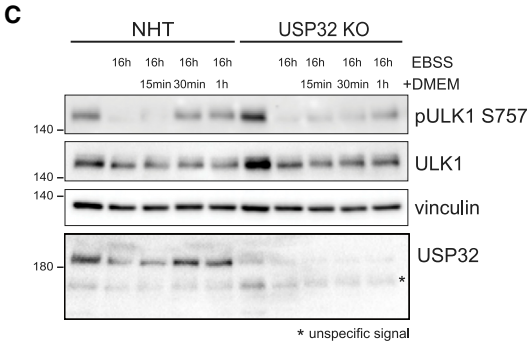

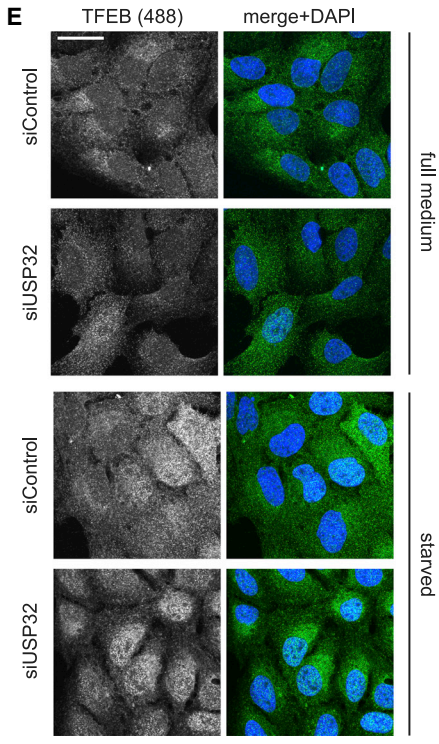

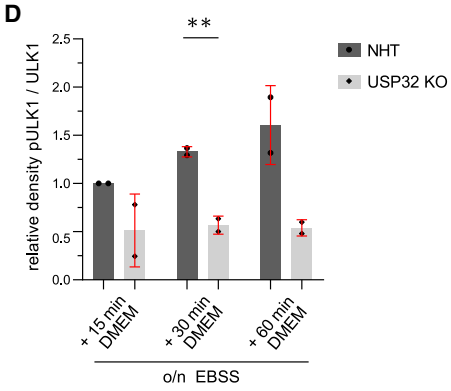

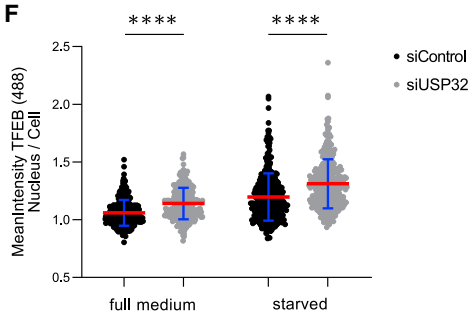

(legend on next page)

(S52), all of which are related to autophagy induction (Figures 5C and S5). Whereas the total protein levels of ULK1 were comparable in both cell lines after starvation and reactivation of mTORC1, phosphorylation was decreased in USP32-deficient cells (Figures 5C and 5D), confirming that in addition to altered localization, mTORC1 activity is also reduced in USP32 KO cells. Complementary, we analyzed intracellular localization of the transcription factor EB (TFEB). Phosphorylation of TFEB by mTORC1 mediates its cytoplasmic retention, whereas inactive mTORC1 allows nuclear translocation of TFEB and activation of target gene expression.[37–39] Knockdown of USP32 caused accumulation of TFEB in the nucleus as compared with cells transfected with non-targeting control siRNAs (Figures 5E and 5F), suggesting reduced mTORC1 activity and TFEB phosphorylation.

Based on the presented data, we propose the following model: USP32 deubiquitinates the Ragulator complex component LAMTOR1, it cleaves non-proteolytic ubiquitin signals conjugated to K20. LAMTOR1 deubiquitination is a prerequisite for efficient interaction between Ragulator and the lysosomal v-ATPase, and consequently for the subsequent events leading to full mTORC1 activation. In the absence of USP32, ubiquitinated LAMTOR1 accumulates, which results in weaker binding to v-ATPase, altered mTORC1 positioning to the lysosome, and reduced activation of the kinase complex. In addition to regulating LAMTOR1 protein levels by UBE3A-mediated proteasomal degradation,[34] we present evidence that USP32-sensitive, non-proteolytic ubiquitination of LAMTOR1 impacts Ragulator function by regulating the interaction between LAMTOR1 and the lysosomal v-ATPase.

USP32 regulates mTOR-TFEB-autophagy axis in *Caenorhabditis elegans*

To investigate if USP32-dependent regulation of autophagy is evolutionarily conserved, we included the nematode *Caenorhabditis elegans* in our studies. We depleted the USP32 homolog CYK-3 in worms expressing the ubiquitin-like modifier GFP:LGG1, the homolog of human GABARAP. Knockdown of CYK-3 by RNAi resulted in an accumulation of GFP-LGG1 puncta in the dermis of one-day adult worms as compared with control RNAi worms (Figures 6A and 6B), suggesting increased autophagy. While treatment with the mTORC1 inhibitor metformin caused a strong increase in GFP-LGG1 puncta in control animals, no further increase in GFP-LGG1 puncta was detected in CYK-3-depleted animals, indicating that autophagy was already strongly activated and mTORC1 inhibited by CYK-3 knockdown (Figures 6C and 6D). To further investigate the consequence of reduced mTORC1 activity, subcellular localization of the *C. elegans* TFEB homolog HLH-30 was analyzed in intestinal cells. In control animals, HLH-30-GFP showed a mainly diffuse cytosolic localization, while TORC1 inactivation through metformin lead to a strong nuclear translocation of HLH-30-GFP. A comparable HLH-30-GFP nuclear localization was observed in CYK-3 RNAi animals without metformin treatment, indicating that TORC1 signaling is impaired in CYK-3 knockdown animals.

DISCUSSION

Amino acid-mediated regulation of mTORC1 activation requires a lysosome-based platform consisting of multiple proteins, among which is the Ragulator complex. LAMTOR1 is critical for Ragulator-Rag GTPase complex stabilization and its anchoring to lysosomes.[41] Here, we describe a mechanism how Ragulator function at the lysosomal membrane is regulated by LAMTOR1 ubiquitination. We show that this non-proteolytic ubiquitin signal in turn is terminated by the rather enigmatic ubiquitin-specific protease USP32. By controlling the ubiquitination status of at least two proteins of the endosomal-lysosomal system, USP32 eventually impacts autophagic substrate degradation in human cells. Complementary, we demonstrate that depletion of the USP32 homolog CYK-3 in *C. elegans* results in mTOR inhibition and autophagy induction.

Driven by the aim to characterize the physiological function of USP32 we used an unbiased SILAC-based ubiquitin-modified proteome analysis and revealed multiple proteins of the endosomal-lysosomal system that are hyperubiquitinated in USP32 KO cells. First, we focused on the small GTPase Rab7, given its critical role in endosome maturation and membrane trafficking.[13] Loss of USP32 increased ubiquitination of Rab7 at K191/194, which enhanced binding of Rab7 to its effector protein RILP and accelerated retrograde transport of CI-MPR. Previously, the E3 ubiquitin ligase Parkin was reported to preferentially ubiquitinate Rab7 at K38, which promotes both Rab7 localization at LEs and its interaction with RILP.[26] Rab7 positioning at membranes and binding of effectors is mediated by C-terminal prenylation of Rab7 and its nucleotide status. Activation of Rab7 is tightly regulated by the cooperation of GEFs and GTPase activating proteins (GAPs), as well as GDP dissociation inhibitors (GDIs).[42] In our study, hyperubiquitination of Rab7 at K191/194 did not change the overall localization of Rab7, suggesting that prenylation and membrane recruitment of Rab7 is not impaired.

Figure 5. LAMTOR1 ubiquitination reduces mTORC1 recruitment and activation

(A) Lysosomal localization of mTOR is partially lost in USP32 KO cells. Representative immunofluorescence microscopy images of mTOR and LAMP2 co-staining in untreated and 2 h amino acid-starved RPE1 NHT and USP32 KO cells. Scale bar, 20 μm.

(B) Quantification of mTOR colocalization to LAMP2 positive structures shown as Pearson's coefficient (per cell) with indicated mean ± SD, $^{**}p < 0.01$, $^{***}p < 0.001$, unpaired Student's t test (n = 3).

(C) Phosphorylation of mTORC1 substrate ULK1 is decreased after reactivation in USP32 KO cells. RPE1 NHT and USP32 KO cells were amino acid-starved for 16 h (EBSS medium) and subsequently cultured in full medium (DMEM) for the indicated time points. Protein levels were detected by western blotting.

(D) Relative quantification of immunoblot of pULK1 S757 normalized to total ULK1 level from (C), $^{**}p < 0.01$, unpaired Student's t test (n = 2).

(E) TFEB translocation to the nucleus is increased in USP32 KD cells. Representative immunofluorescence microscopy images of endogenous TFEB in untreated and 4 h amino acid-starved U2OS cells transfected with siControl or siUSP32 pool. Scale bar, 20 μm.

(F) Quantification of TFEB translocation shown as ratio of mean intensity in nucleus and whole cell (per cell) with indicated mean ± SD, $^{****}p < 0.0001$, unpaired Student's t test (n = 2). See also Figure S5.

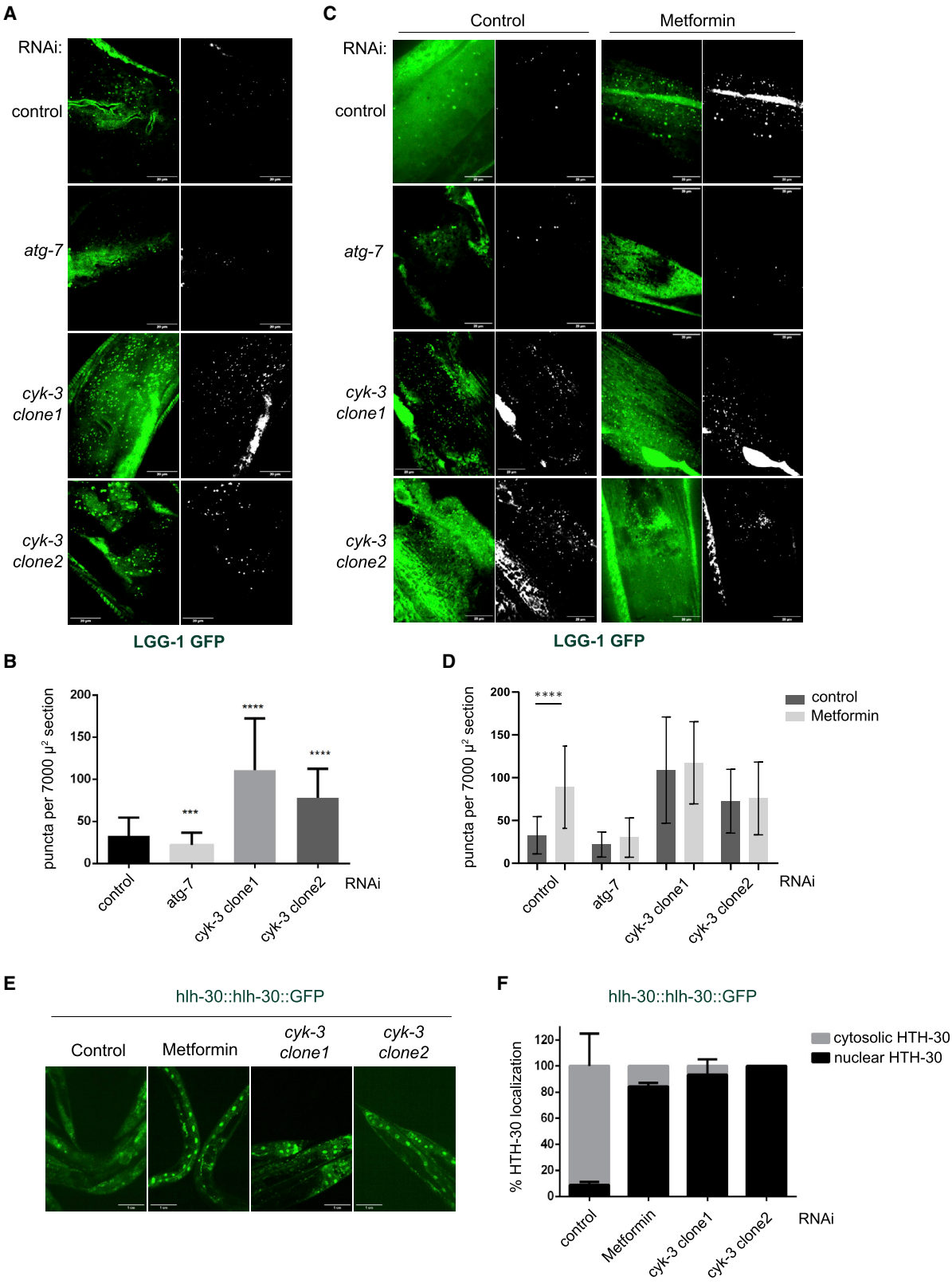

(legend on next page)

However, we observed a stronger interaction between Rab7 and RILP in the absence of USP32, raising the possibility that either the affinity of Rab7 for RILP or the activity of Rab7 regulated by GEFs and GAPs is altered by USP32-sensitive ubiquitination. A crystal structure of Rab7-GTP in complex with the Rab7 binding domain of RILP[43] shows that the ubiquitination sites K38 and K191/194 of Rab7 are either directly within or in close proximity to the surface bound by RILP, supporting the hypothesis that USP32-regulated ubiquitin signals directly fine-tune interaction between both proteins.

A recent study by Ovaa and colleagues also described Rab7 as substrate of USP32.[10] In contrast to our data, they observed a dramatic relocalization of Rab7 to membranes in the periphery and an inhibition of LE transport and recycling of LE cargos in USP32-deficient cells, as well as increased binding of RILP to an ubiquitination-deficient Rab7 mutant. Possible reasons for the discrepancy could be the use of different cell models and depletion methods (melanoma MelJuSo cells and cervix carcinoma HeLa cells, siRNA[11] versus hTERT-immortalized primary RPE1 cells, CRISPR-Cas). However, both studies demonstrate that USP32-regulated ubiquitination of Rab7 impacts function of this central small GTPase by modulating binding to effector proteins. Our data show in addition that loss of USP32 induces autophagy. This observation prompted us to further investigate other potential USP32 substrates that could link USP32-sensitive ubiquitination to autophagy. LAMTOR1 was a promising candidate and we show that USP32 indeed counteracts LAMTOR1 ubiquitination, specifically at K20. Our work establishes that accumulation of this ubiquitin signal weakens LAMTOR1 interaction with the lysosomal v-ATPase. This evolutionarily conserved ATP-driven rotary proton pump couples ATP hydrolysis by its peripheral V1 domain to proton translocation through the membrane integral V0 domain to acidify the lysosome, hence enabling its degradative functions.[44,45] The v-ATPase forms a complex with Ragulator and the Rag GTPases, and its integrity and activity are essential for lysosomal mTORC1 recruitment in response to amino acids.[46,47] Interestingly, a small-molecule activator of autophagy has been identified (EN6), which acts through covalent targeting of a regulatory cysteine on the v-ATPase subunit ATP6V1A. EN6 decouples the v-ATPase from the Rags, leading to inhibition of mTORC1 signaling, increased lysosomal acidification and activation of autophagy.[48] This study highlights that interfering with the function of v-ATPase and its interaction with Ragulator specifically induces autophagy. Thus, we conclude that hyperubiquitinated LAMTOR1 and its consequences on v-ATPase binding are at least one reason for autophagy activation in USP32 KO cells.

Recently, the E3 ubiquitin ligase UBE3A was shown to target LAMTOR1 for proteasomal degradation, mainly through ubiquitinating K60, K103 and K104.[33] UBE3A limits mTORC1 signaling and activity-dependent synaptic remodeling, and maternal UBE3A deficiency results in Angelman syndrome (AS).[49] In the absence of UBE3A, LAMTOR1 accumulates in neurons, resulting in mTORC1 overactivation, abnormal synaptic morphology, and impaired synaptic plasticity and learning.[34] In addition to UBE3A-mediated regulation of LAMTOR1 protein turnover, we identify a second layer of negative regulation of the Ragulator complex by non-proteolytic ubiquitination of LAMTOR1 at K20. For efficient interaction between Ragulator and v-ATPase, LAMTOR1 needs to be deubiquitinated by USP32.

Another ubiquitin-dependent control layer of mTORC1 activation, independent of Ragulator and the v-ATPase, was described by Inoki and colleagues.[23] Their work revealed that amino acids stimulate polyubiquitination of the small GTPase Rheb, which in turn enhances its binding preference for mTORC1 and thus promotes activation of the kinase complex. Interestingly, in amino acid-starved conditions, the deubiquitinase Ataxin 3 is recruited to lysosomes where it contributes to mTORC1 inactivation by terminating Rheb ubiquitination,[23] again highlighting how signaling events are regulated by cooperation of E3 ubiquitin ligases and DUBs.

Interestingly, although we observed reduced ULK1 S757 phosphorylation in USP32 KO cells and also accumulation of nuclear TFEB as a consequence of reduced mTORC1 activity, activation of the well-characterized mTORC1 substrates S6K1 and 4EBP1 was not altered in the absence of USP32. Spatial regulation of mTORC1 substrates could contribute to their differential phosphorylation. Another possibility could be a threshold of activated kinase that has not been undercut by USP32 KO to prevent mTORC1 substrate phosphorylation completely. Our data suggest that LAMTOR1 ubiquitination prevents efficient interaction with v-ATPase and this negatively affects Ragulator function

Figure 6. RNAi knockdown of the *C. elegans* USP32 ortholog CYK-3 leads to autophagy induction due to mTOR inhibition

(A) Inactivation of CYK-3 by RNAi leads to an accumulation of GFP-LGG-1 puncta in the epidermis of 1-day adults animals as compared with control RNAi animals. In contrast, inactivation of the autophagy initiation factor ATG-7 leads to a reduction of GFP-LGG-1 puncta. For CYK-3 RNAi two different RNAi clones were used corresponding to the 5′ and 3′ part of the cyk-3 cDNA, respectively. Shown are maximum intensity projections (left) as well as binarized black and white images after thresholding (right). Scale bar, 20 μm.

(B) Quantification of GFP-LGG-1 puncta, the mean ± SEM are shown.

(C) Images show the accumulation of GFP-LGG-1 puncta after metformin treatment of the RNAi animals. In control RNAi animals, metformin treatment leads to a strong accumulation of GFP-LGG-1 puncta, while ATG-7 RNAi largely prevents the formation of GFP-LGG-1 puncta in untreated and metformin-treated animals. Metformin treatment in cyk-3 RNAi animals does not lead to a further increase of GFP-LGG-1 puncta compared with the untreated situation. This suggests that autophagy is already strongly activated through RNAi knockdown of CYK-3. Scale bar, 20 μm.

(D) Quantification of GFP-LGG1 puncta shown in (C) (mean ± SEM, two-sided Student's t test, ****$p < 0.0001$).

(E) Images showing subcellular localization of the *C. elegans* TFEB homolog HLH-30 in intestinal cells. In control RNAi HLH-30-GFP showed a mainly diffuse cytosolic localization, while TORC1 inactivation through metformin[40] leads to a strong nuclear translocation of HLH-30-GFP. A similar HLH-30-GFP nuclear localization is also seen in cyk-3 RNAi animals without metformin treatment. This suggests that TORC1 signaling is largely inactivated in CYK-3 knockdown animals. Scale bar, 1 cm.

(F) The quantification of the nuclear localization of HLH-30-GFP is shown in cyk-3 RNAi and metformin-treated animals as compared with the control RNAi (mean ± SEM).

and full mTORC1 activation. Since it not entirely abrogates kinase activation, it is possible that substrates are not equally sensitive to or affected by these changes.

Depletion of USP32 in RPE1 cells results in elevated autophagy. The above described USP32 substrates Rab7 and LAMTOR1 have both been linked to the autophagy pathway, and altered functions of these proteins in USP32 KO cells probably both contribute to the autophagy phenotype. However, loss of USP32 may impact autophagic substrate degradation on further levels. For example, USP32 interacts with VPS35,[27] a component of the mammalian retromer complex. In addition to the well-documented role of retromer in the endocytic recycling of transmembrane proteins from endosomes back to the cell surface and to the TGN,[50–52] retromer is also required to maintain lysosomal amino acid signaling through mTORC1.[53] In retromer-defective cells, amino acids no longer stimulate mTORC1 translocation to the lysosomal membrane, which leads to a loss of mTORC1 activity and increased induction of autophagy.

Besides Rab7 and LAMTOR1, additional proteins of the endosomal-lysosomal system were identified as possible USP32 substrates, for example TMEM192, which was discovered in 2010 as a lysosomal transmembrane protein.[54] Depletion of TMEM192 in normal mouse tissue has no significant effect, whereas it induces apoptosis and autophagy in HepG2 hepatoma cells.[55,56] Recent studies identified TMEM192 to be ubiquitinated upon lysosomal damage.[57] It would be interesting to further investigate the role of USP32-sensitive ubiquitination in the context of lysosomal damage repair and lysophagy.

Taken together, we identified USP32 as versatile regulator in the endosomal-lysosomal system. Our data show that USP32 controls ubiquitin signals at small GTPases and lysosomal or lysosome-associated proteins, ultimately ensuring cellular homeostasis by securing correct translocation and activation of mTORC1 to lysosomes and autophagy induction.

Limitations of the study

Although we identified USP32-regulated ubiquitination of Rab7 and LAMTOR1 and present functional consequences of these ubiquitin signals *in cellulo* and the model organism *C. elegans* by using constitutive knockout and transient knockdown strategies, our study does not provide *in vitro* data demonstrating a direct deubiquitination of, e.g., LAMTOR1 at K20. It will be important to also include mutant LAMTOR1 (K20R) or Rab7 (K191/194R) to further prove a direct functional correlation between these ubiquitination sites and the observed phenotypes.

The E3 ligase UBE3A has been shown to target LAMTOR1 for proteasomal degradation.[34] Future aims include identification of the E3 ligase that modifies LAMTOR1 at K20 and thereby regulates interaction with other proteins. Furthermore, structural studies have the potential to reveal the effect of ubiquitination within LAMTOR1's N-terminal, unstructured region and the impact on engaging with binding partners.

STAR★METHODS

Detailed methods are provided in the online version of this paper and include the following:

- KEY RESOURCES TABLE
- RESOURCE AVAILABILITY
  - Lead contact
  - Materials availability
  - Data and code availability
- EXPERIMENTAL MODEL AND SUBJECT DETAILS
- METHOD DETAILS
  - Cell transfection & treatment
  - Cell lysis and immunoblotting
  - Antibodies
  - Immunofluorescence staining and confocal microscopy
  - Flow cytometry
  - Subcellular fractionation
  - CI-MPR uptake assays
  - RILP assay
  - His-Ubiquitin pulldown
  - TUBE PD
  - LAMTOR1-GFP immunoprecipitation
  - Interactome and GlyGly-Site analysis
  - Co-immunoprecipitation
  - Ubiquitin-modified proteome analysis (diGly remnant profiling)
  - Lysosome enrichment
  - Lysosome proteome
  - Guide RNA design and CRISPR/Cas9 plasmid generation
  - Generation of high titer lentivirus and viral transduction
  - DNA and siRNA constructs
  - *C. elegans* RNA interference and drug treatment
  - *C. elegans* live-cell imaging microscopy
- QUANTIFICATION AND STATISTICAL ANALYSIS

SUPPLEMENTAL INFORMATION

Supplemental information can be found online at https://doi.org/10.1016/j.celrep.2022.111653.

ACKNOWLEDGMENTS

We thank Sylvie Urbé and Ayse E. Erson for USP32 constructs, Bernd Schröder for anti-TMEM192 antibody, Tassula Proikas-Cezanne for anti-pWIPI2 (S413) antibody, and the Quantitative Proteomics Unit at IBC2 (Goethe University, Frankfurt) for providing technical support. This work was funded by the Deutsche Forschungsgemeinschaft (DFG, German Research Foundation) – Project ID 323732846 and Project ID 25913077-SFB 1177.

AUTHOR CONTRIBUTIONS

Conceptualization, A.B.; Methodology, A.H., L.M.A., F.B., G.T., M.K., S.E., and F.S.; Formal Analysis, A.H., F.B., G.T., and F.S.; Investigation, A.H., L.M.A., H.D., and F.S., Resources, I.D., M.K.; Data Curation, A.H., F.B., and G.T.; Writing – Original Draft, A.B.; Writing Review & Editing, A.H., I.D., S.E., F.S., and A.B.; Visualization, A.H., S.E., F.S., and A.B.; Supervision, A.B.; Funding Acquisition, A.B.

DECLARATION OF INTERESTS

The authors declare no competing interests.

INCLUSION AND DIVERSITY

We support inclusive, diverse, and equitable conduct of research.

Received: January 18, 2022
Revised: August 16, 2022
Accepted: October 20, 2022
Published: December 6, 2022

REFERENCES

1. Perez-Riverol, Y., Csordas, A., Bai, J., Bernal-Llinares, M., Hewapathirana, S., Kundu, D.J., Inuganti, A., Griss, J., Mayer, G., Eisenacher, M., et al. (2019). The PRIDE database and related tools and resources in 2019: improving support for quantification data. Nucleic Acids Res. *47*, D442–D450.
2. Akimov, V., Barrio-Hernandez, I., Hansen, S.V.F., Hallenborg, P., Pedersen, A.-K., Bekker-Jensen, D.B., Puglia, M., Christensen, S.D.K., Vanselow, J.T., Nielsen, M.M., et al. (2018). UbiSite approach for comprehensive mapping of lysine and N-terminal ubiquitination sites. Nat. Struct. Mol. Biol. *19*, 886.
3. Oh, E., Akopian, D., and Rape, M. (2018). Principles of ubiquitin-dependent signaling. Annu. Rev. Cell Dev. Biol. *34*, 137–162.
4. Harrigan, J.A., Jacq, X., Martin, N.M., and Jackson, S.P. (2017). Deubiquitylating enzymes and drug discovery: emerging opportunities. Nat. Rev. Drug Discov., 1–21.
5. Schauer, N.J., Magin, R.S., Liu, X., Doherty, L.M., and Buhrlage, S.J. (2020). Advances in discovering deubiquitinating enzyme (DUB) inhibitors. J. Med. Chem. *63*, 2731–2750.
6. Clague, M.J., Urbé, S., and Komander, D. (2019). Breaking the chains: deubiquitylating enzyme specificity begets function. Nat. Rev. Mol. Cell Biol. *20*, 338–352.
7. Akhavantabasi, S., Akman, H.B., Sapmaz, A., Keller, J., Petty, E.M., and Erson, A.E. (2010). USP32 is an active, membrane-bound ubiquitin protease overexpressed in breast cancers. Mamm. Genome *21*, 388–397.
8. Hu, W., Wei, H., Li, K., Li, P., Lin, J., and Feng, R. (2017). Downregulation of USP32 inhibits cell proliferation, migration and invasion in human small cell lung cancer. Cell Prolif *50*.
9. Dou, N., Hu, Q., Li, L., Wu, Q., Li, Y., and Gao, Y. (2020). USP32 promotes tumorigenesis and chemoresistance in gastric carcinoma via upregulation of SMAD2. Int. J. Biol. Sci. *16*, 1648–1657.
10. Nakae, A., Kodama, M., Okamoto, T., Tokunaga, M., Shimura, H., Hashimoto, K., Sawada, K., Kodama, T., Copeland, N.G., Jenkins, N.A., et al. (2021). Ubiquitin specific peptidase 32 acts as an oncogene in epithelial ovarian cancer by deubiquitylating farnesyl-diphosphate farnesyltransferase 1. Biochem. Biophys. Res. Commun. *552*, 120–127.
11. Sapmaz, A., Berlin, I., Bos, E., Wijdeven, R.H., Janssen, H., Konietzny, R., Akkermans, J.J., Erson-Bensan, A.E., Koning, R.I., Kessler, B.M., et al. (2019). USP32 regulates late endosomal transport and recycling through deubiquitylation of Rab7. Nat. Commun. *10*, 1454.
12. Huotari, J., and Helenius, A. (2011). Endosome maturation. EMBO J. *30*, 3481–3500.
13. Langemeyer, L., Fröhlich, F., and Ungermann, C. (2018). Rab GTPase function in endosome and lysosome biogenesis. Trends Cell Biol. *28*, 957–970.
14. Modica, G., and Lefrancois, S. (2017). Post-translational modifications: how to modulate Rab7 functions. Small GTPases *13*, 1–7.
15. Ballabio, A., and Bonifacino, J.S. (2020). Lysosomes as dynamic regulators of cell and organismal homeostasis. Nat. Rev. Mol. Cell Biol. *21*, 101–118.
16. Liu, G.Y., and Sabatini, D.M. (2020). mTOR at the nexus of nutrition, growth, ageing and disease. Nat. Rev. Mol. Cell Biol. *21*, 183–203.
17. Sancak, Y., Bar-Peled, L., Zoncu, R., Markhard, A.L., Nada, S., and Sabatini, D.M. (2010). Ragulator-Rag complex targets mTORC1 to the lysosomal surface and is necessary for its activation by amino acids. Cell *141*, 290–303.
18. Wang, S., Tsun, Z.-Y., Wolfson, R.L., Shen, K., Wyant, G.A., Plovanich, M.E., Yuan, E.D., Jones, T.D., Chantranupong, L., Comb, W., et al. (2015). Metabolism. Lysosomal amino acid transporter SLC38A9 signals arginine sufficiency to mTORC1. Science *347*, 188–194.
19. Rebsamen, M., Pochini, L., Stasyk, T., de Araújo, M.E.G., Galluccio, M., Kandasamy, R.K., Snijder, B., Fauster, A., Rudashevskaya, E.L., Bruckner, M., et al. (2015). SLC38A9 is a component of the lysosomal amino acid sensing machinery that controls mTORC1. Nature *519*, 477–481.
20. Jung, J., Genau, H.M., and Behrends, C. (2015). Amino acid-dependent mTORC1 regulation by the lysosomal membrane protein SLC38A9. Mol. Cell Biol. *35*, 2479–2494.
21. Bar-Peled, L., Schweitzer, L.D., Zoncu, R., and Sabatini, D.M. (2012). Ragulator is a GEF for the Rag GTPases that signal amino acid levels to mTORC1. Cell *150*, 1196–1208.
22. de Araújo, M.E.G., Stasyk, T., Taub, N., Ebner, H.L., Fürst, B., Filipek, P., Weys, S.R., Hess, M.W., Lindner, H., Kremser, L., et al. (2013). Stability of the endosomal scaffold protein LAMTOR3 depends on heterodimer assembly and proteasomal degradation. J. Biol. Chem. *288*, 18228–18242.
23. Yao, Y., Hong, S., Ikeda, T., Mori, H., MacDougald, O.A., Nada, S., Okada, M., and Inoki, K. (2020). Amino acids enhance polyubiquitination of Rheb and its binding to mTORC1 by blocking lysosomal ATXN3 deubiquitinase activity. Mol. Cell *80*, 437–451.
24. Hu, J., Zacharek, S., He, Y.J., Lee, H., Shumway, S., Duronio, R.J., and Xiong, Y. (2008). WD40 protein FBW5 promotes ubiquitination of tumor suppressor TSC2 by DDB1-CUL4-ROC1 ligase. Genes Dev. *22*, 866–871.
25. Guerra, F., and Bucci, C. (2016). Multiple roles of the small GTPase Rab7. Cells *5*, 28–34.
26. Song, P., Trajkovic, K., Tsunemi, T., and Krainc, D. (2016). Parkin modulates endosomal organization and function of the endo-lysosomal pathway. J. Neurosci. *36*, 2425–2437.
27. Sun, J., Deghmane, A.-E., Bucci, C., and Hmama, Z. (2009). Detection of activated Rab7 GTPase with an immobilized RILP probe. In Methods in Molecular Biology, pp. 57–69.
28. Sowa, M.E., Bennett, E.J., Gygi, S.P., and Harper, J.W. (2009). Defining the human deubiquitinating enzyme interaction landscape. Cell *138*, 389–403.
29. Seaman, M.N.J. (2021). The retromer complex: from genesis to Revelations. Trends Biochem. Sci. *46*, 608–620.
30. Jager, S., Bucci, C., Tanida, I., Ueno, T., Kominami, E., Saftig, P., and Eskelinen, E.-L. (2004). Role for Rab7 in maturation of late autophagic vacuoles. J. Cell Sci. *117*, 4837–4848.
31. Klionsky, D.J., Abdel-Aziz, A.K., Abdelfatah, S., Abdellatif, M., Abdoli, A., Abel, S., Abeliovich, H., Abildgaard, M.H., Abudu, Y.P., Acevedo-Arozena, A., et al. (2021). Guidelines for the use and interpretation of assays for monitoring autophagy. Autophagy *10*.
32. Hannus, M., Beitzinger, M., Engelmann, J.C., Weickert, M.-T., Spang, R., Hannus, S., and Meister, G. (2014). siPools: highly complex but accurately defined siRNA pools eliminate off-target effects. Nucleic Acids Res. *42*, 8049–8061.
33. Kaizuka, T., Morishita, H., Hama, Y., Tsukamoto, S., Matsui, T., Toyota, Y., Kodama, A., Ishihara, T., Mizushima, T., and Mizushima, N. (2016). An autophagic flux probe that Releases an internal control. Mol. Cell *64*, 835–849.
34. Sun, J., Liu, Y., Jia, Y., Hao, X., Lin, W.J., Tran, J., Lynch, G., Baudry, M., and Bi, X. (2018). UBE3A-mediated p18/LAMTOR1 ubiquitination and degradation regulate mTORC1 activity and synaptic plasticity. Elife *7*.
35. Sanders, S.S., De Simone, F.I., and Thomas, G.M. (2019). mTORC1 signaling is palmitoylation-dependent in hippocampal neurons and

non-neuronal cells and involves dynamic palmitoylation of LAMTOR1 and mTOR. Front. Cell. Neurosci. *13*, 115.

36. Hjerpe, R., Aillet, F., Lopitz-Otsoa, F., Lang, V., England, P., and Rodriguez, M.S. (2009). Efficient protection and isolation of ubiquitylated proteins using tandem ubiquitin-binding entities. EMBO Rep. *10*, 1250–1258.
37. Settembre, C., Zoncu, R., Medina, D.L., Vetrini, F., Erdin, S., Erdin, S., Huynh, T., Ferron, M., Karsenty, G., Vellard, M.C., et al. (2012). A lysosome-to-nucleus signalling mechanism senses and regulates the lysosome via mTOR and TFEB. EMBO J. *31*, 1095–1108.
38. Martina, J.A., Chen, Y., Gucek, M., and Puertollano, R. (2012). MTORC1 functions as a transcriptional regulator of autophagy by preventing nuclear transport of TFEB. Autophagy *8*, 903–914.
39. Roczniak-Ferguson, A., Petit, C.S., Froehlich, F., Qian, S., Ky, J., Angarola, B., Walther, T.C., and Ferguson, S.M. (2012). The transcription factor TFEB links mTORC1 signaling to transcriptional control of lysosome homeostasis. Sci. Signal. *5*.
40. Chen, J., Ou, Y., Li, Y., Hu, S., Shao, L.-W., and Liu, Y. (2017). Metformin extends C. elegans lifespan through lysosomal pathway. Elife *6*.
41. Nada, S., Hondo, A., Kasai, A., Koike, M., Saito, K., Uchiyama, Y., and Okada, M. (2009). The novel lipid raft adaptor p18 controls endosome dynamics by anchoring the MEK-ERK pathway to late endosomes. EMBO J. *28*, 477–489.
42. Müller, M.P., and Goody, R.S. (2018). Molecular control of Rab activity by GEFs, GAPs and GDI. Small GTPases *9*, 5–21.
43. Wu, M., Wang, T., Loh, E., Hong, W., and Song, H. (2005). Structural basis for recruitment of RILP by small GTPase Rab7. EMBO J. *24*, 1491–1501.
44. Forgac, M. (2007). Vacuolar ATPases: rotary proton pumps in physiology and pathophysiology. Nat. Rev. Mol. Cell Biol. *8*, 917–929.
45. Zhao, J., Benlekbir, S., and Rubinstein, J.L. (2015). Electron cryomicroscopy observation of rotational states in a eukaryotic V-ATPase. Nature *521*, 241–245.
46. Zoncu, R., Bar-Peled, L., Efeyan, A., Wang, S., Sancak, Y., and Sabatini, D.M. (2011). mTORC1 senses lysosomal amino acids through an inside-out mechanism that requires the vacuolar H(+)-ATPase. Science *334*, 678–683.
47. Jewell, J.L., Kim, Y.C., Russell, R.C., Yu, F.-X., Park, H.W., Plouffe, S.W., Tagliabracci, V.S., and Guan, K.-L. (2015). Metabolism. Differential regulation of mTORC1 by leucine and glutamine. Science *347*, 194–198.
48. Chung, C.Y.-S., Shin, H.R., Berdan, C.A., Ford, B., Ward, C.C., Olzmann, J.A., Zoncu, R., and Nomura, D.K. (2019). Covalent targeting of the vacuolar H+-ATPase activates autophagy via mTORC1 inhibition. Nat. Chem. Biol. *15*, 776–785.
49. Williams, C.A., Zori, R.T., Stone, J.W., Gray, B.A., Cantu, E.S., and Ostrer, H. (1990). Maternal origin of 15q11-13 deletions in Angelman syndrome suggests a role for genomic imprinting. Am. J. Med. Genet. *35*, 350–353.
50. Steinberg, F., Gallon, M., Winfield, M., Thomas, E.C., Bell, A.J., Heesom, K.J., Tavaré, J.M., and Cullen, P.J. (2013). A global analysis of SNX27–retromer assembly and cargo specificity reveals a function in glucose and metal ion transport. Nat. Cell Biol. *15*, 461–471.
51. Arighi, C.N., Hartnell, L.M., Aguilar, R.C., Haft, C.R., and Bonifacino, J.S. (2004). Role of the mammalian retromer in sorting of the cation-independent mannose 6-phosphate receptor. J. Cell Biol. *165*, 123–133.
52. Seaman, M.N.J. (2004). Cargo-selective endosomal sorting for retrieval to the Golgi requires retromer. J. Cell Biol. *165*, 111–122.
53. Kvainickas, A., Nägele, H., Qi, W., Dokládal, L., Jimenez-Orgaz, A., Stehl, L., Gangurde, D., Zhao, Q., Hu, Z., Dengjel, J., et al. (2019). Retromer and TBC1D5 maintain late endosomal RAB7 domains to enable amino acid–induced mTORC1 signaling. J. Cell Biol. *218*, 3019–3038.
54. Schröder, B., Wrocklage, C., Hasilik, A., and Saftig, P. (2010). Molecular characterisation of "transmembrane protein 192" (TMEM192), a novel protein of the lysosomal membrane. Biol. Chem. *391*, 695–704.
55. Liu, Z., Lv, Y.J., Song, Y.P., Li, X.H., Du, Y.N., Wang, C.H., and Hu, L.K. (2012). Lysosomal membrane protein TMEM192 deficiency triggers crosstalk between autophagy and apoptosis in HepG2 hepatoma cells. Oncol. Rep. *28*, 985–991.
56. Nguyen, T.L., Schneppenheim, J., Rudnik, S., Lüllmann-Rauch, R., Bernreuther, C., Hermans-Borgmeyer, I., Glatzel, M., Saftig, P., and Schröder, B. (2017). Functional characterization of the lysosomal membrane protein TMEM192 in mice. Oncotarget *8*, 43635–43652.
57. Yoshida, Y., Yasuda, S., Fujita, T., Hamasaki, M., Murakami, A., Kawawaki, J., Iwai, K., Saeki, Y., Yoshimori, T., Matsuda, N., et al. (2017). Ubiquitination of exposed glycoproteins by SCF FBXO27 directs damaged lysosomes for autophagy. Proc. Natl. Acad. Sci. *114*, 8574–8579.
58. Brenner, S. (1974). The genetics od Caenorhabditis elegans. Genetics *77*, 71–94.
59. Kang, C., You, Y., and Avery, L. (2007). Dual roles of autophagy in the survival of Caenorhabditis elegans during starvation. Genes Dev. *21*, 2161–2171.
60. Lapierre, L.R., De Magalhaes Filho, C.D., McQuary, P.R., Chu, C.-C., Visvikis, O., Chang, J.T., Gelino, S., Ong, B., Davis, A.E., Irazoqui, J.E., et al. (2013). The TFEB orthologue HLH-30 regulates autophagy and modulates longevity in Caenorhabditis elegans. Nat. Commun. *4*, 2267.
61. Schneider, C.A., Rasband, W.S., and Eliceiri, K.W. (2012). NIH Image to ImageJ: 25 years of image analysis. Nat. Methods *9*, 671–675.
62. McQuin, C., Goodman, A., Chernyshev, V., Kamentsky, L., Cimini, B.A., Karhohs, K.W., Doan, M., Ding, L., Rafelski, S.M., Thirstrup, D., et al. (2018). CellProfiler 3.0: next-generation image processing for biology. PLoS Biol. *16*, e2005970.
63. Cox, J., Neuhauser, N., Michalski, A., Scheltema, R.A., Olsen, J.V., and Mann, M. (2011). Andromeda: a peptide search engine integrated into the MaxQuant environment. J. Proteome Res. *10*, 1794–1805.
64. Tyanova, S., Temu, T., and Cox, J. (2016). The MaxQuant computational platform for mass spectrometry-based shotgun proteomics. Nat. Protoc. *11*, 2301–2319.
65. Elias, J.E., and Gygi, S.P. (2007). Target-decoy search strategy for increased confidence in large-scale protein identifications by mass spectrometry. Nat. Methods *4*, 207–214.
66. Cox, J., Hein, M.Y., Luber, C.A., Paron, I., Nagaraj, N., and Mann, M. (2014). Accurate proteome-wide label-free quantification by delayed normalization and maximal peptide ratio extraction, termed MaxLFQ. Mol. Cell. Proteomics *13*, 2513–2526.
67. Tyanova, S., Temu, T., Sinitcyn, P., Carlson, A., Hein, M.Y., Geiger, T., Mann, M., and Cox, J. (2016). The Perseus computational platform for comprehensive analysis of (prote)omics data. Nat. Methods *13*, 731–740.
68. Doench, J.G., Fusi, N., Sullender, M., Hegde, M., Vaimberg, E.W., Donovan, K.F., Smith, I., Tothova, Z., Wilen, C., Orchard, R., et al. (2016). Optimized sgRNA design to maximize activity and minimize off-target effects of CRISPR-Cas9. Nat. Biotechnol. *34*, 184–191.
69. Hammell, C.M., and Hannon, G.J. (2012). Inducing RNAi in C. elegans by feeding with dsRNA-expressing E. coli. Cold Spring Harb. Protoc. *2012*, pdb.prot072348.
70. Gomes, L.C., Odedra, D., Dikic, I., and Pohl, C. (2016). Autophagy and modular restructuring of metabolism control germline tumor differentiation and proliferation in C. elegans. Autophagy *12*, 529–546.
71. Schindelin, J., Arganda-Carreras, I., Frise, E., Kaynig, V., Longair, M., Pietzsch, T., Preibisch, S., Rueden, C., Saalfeld, S., Schmid, B., et al. (2012). Fiji: an open-source platform for biological-image analysis. Nat. Methods *9*, 676–682.

STAR★METHODS

KEY RESOURCES TABLE

REAGENT or RESOURCE	SOURCE	IDENTIFIER
Antibodies		
Rabbit anti-ATP6V1A	Abcam	Cat#ab199326, RRID:AB_2802119
Rabbit anti-M6PR, cation independent	Abcam	Cat#ab124767, RRID:AB_10974087
Goat anti-VPS35	Abcam	Cat#ab10099, RRID:AB_296841
Mouse anti-WIPI2	Abcam	Cat#ab105459, RRID:AB_10860881
Rabbit anti-VPS29	Sigma-Aldrich	Cat#HPA039748, RRID:AB_10674426
Mouse anti-GM130	BD Biosciences	Cat#610822, RRID:AB_398141
Rabbit anti-ATP6V1B2	Cell Signaling Technology	Cat#14488, RRID:AB_2798496
Rabbit anti-Cathepsin D	Cell Signaling Technology	Cat#2284, RRID:AB_10694258
Rabbit anti-EGFR	Cell Signaling Technology	Cat#2232, RRID:AB_331707
Rabbit anti-Histone H2B	Cell Signaling Technology	Cat#12364, RRID:AB_2714167
Rabbit anti-LAMTOR1	Cell Signaling Technology	Cat#8975, RRID:AB_10860252
Rabbit anti-LC3 A/B	Cell Signaling Technology	Cat#12741, RRID:AB_2617131
Rabbit anti-mTOR	Cell Signaling Technology	Cat#2983, RRID:AB_2105622
Mouse anti-Myc-Tag	Cell Signaling Technology	Cat#2276, RRID:AB_331783
Rabbit anti-phospho-ULK1 (Ser757)	Cell Signaling Technology	Cat#6888, RRID:AB_10829226
Rabbit anti-PARP	Cell Signaling Technology	Cat#9542, RRID:AB_2160739
Rabbit anti-phospho-WIPI2 (Ser413)	Cell Signaling Technology	Cat#13571, RRID:AB_2798259
Rabbit anti-Rab7	Cell Signaling Technology	Cat#9367, RRID:AB_1904103
Rabbit anti-Rab11	Cell Signaling Technology	Cat#5589, RRID:AB_10693925
Rabbit anti-TFEB	Cell Signaling Technology	Cat#37785, RRID:AB_2799119
Rabbit anti-a-Tubulin	Cell Signaling Technology	Cat#2125, RRID:AB_2619646
Rabbit anti-Ubiquitin	Cell Signaling Technology	Cat#3933, RRID:AB_2180538
Rabbit anti-ULK1	Cell Signaling Technology	Cat#8054, RRID:AB_11178668
Mouse anti-LAMP1	DSHB	Cat#h4a3, RRID:AB_2296838
Mouse anti-LAMP2	DSHB	Cat#H4B4, RRID:AB_2134755
Mouse anti-Actin	Sigma-Aldrich	Cat#A4700, RRID:AB_476730
Rabbit anti-phospho-AMBRA1 (Ser52)	Millipore	Cat#ABC80, RRID:AB_2750901
Rabbit anti-USP32	Atlas Antibodies	Cat#HPA044365, RRID:AB_2678914
Mouse anti-Vinculin	Sigma-Aldrich	Cat#V4505, RRID:AB_477617
Mouse anti-VPS26A	Atlas Antibodies	Cat#AMAb90967, RRID:AB_2665739
Goat anti-Cathepsin X/Z/P	R and D Systems	Cat#AF934, RRID:AB_2087676
Mouse anti-AMBRA1	Santa Cruz Biotechnology	Cat#sc-398204, RRID:AB_2861324
Mouse anti-His-Tag	Santa Cruz Biotechnology	Cat#sc-53073, RRID:AB_783791
Horse anti-mouse IgG-HRP	Cell Signaling Technology	Cat#7076, RRID:AB_330924
Goat anti-rabbit IgG-HRP	Cell Signaling Technology	Cat#7074, RRID:AB_2099233
Donkey anti-goat IgG-HRP	Santa Cruz Biotechnology	Cat#sc-2020, RRID:AB_631728
Donkey anti-mouse IgG-HRP	Santa Cruz Biotechnology	Cat#sc-2096, RRID:AB_641168
Goat anti-rabbit IgG-HRP	Santa Cruz Biotechnology	Cat#sc-2054, RRID:AB_631748
Goat anti-mouse IgG Alexa Fluor 647	Molecular Probes	Cat#A-21235, RRID:AB_2535804
Donkey anti-rabbit IgG Alexa Fluor 488	Molecular Probes	Cat#A-21206, RRID:AB_2535792
Donkey anti-rabbit Alexa Fluor 647	Molecular Probes	Cat#A-31573, RRID:AB_2536183
Rabbit anti-TMEM192	gift from Bernd Schröder	Schröder et al., Biol Chem. 2010
Sheep anti-TGN46	AbD Serotec	Cat#AHP500G, RRID:AB_323104

(*Continued on next page*)

Continued

REAGENT or RESOURCE	SOURCE	IDENTIFIER
Mouse anti-GAPDH	Proteintech	Cat#60004-1-Ig, RRID:AB_2107436
Mouse anti-GST (B-14)	Santa Cruz Biotechnology	Cat#sc-138, RRID:AB_627677
Rabbit anti-Giantin	Abcam	Cat#ab80864, RRID:AB_10670397
Mouse anti-CD222	AbD Serotec	Cat#MCA2048, RRID:AB_323432
Bacterial and virus strains		
Stellar	TaKaRa (Clontech)	Cat#636763
HT115(DE3)	Caenorhabditis Genetics Center; Ref.: Hammell C.M. & Hannon G.J., 2012	N/A
BL21(DE3)	Sigma-Aldrich	Cat#69450
Chemicals, peptides, and recombinant proteins		
EBSS	Thermo Fisher Scientific/Gibco	Cat#24010
MG132	Sigma-Aldrich	Cat#C2211
Bafilomycin A1	LC Laboratories	Cat#B-1080
Polyethylenimine, linear	Polysciences Europe	Cat#23966-2
Lipofectamine RNAiMAX	Invitrogen	Cat#13778075
Ni-NTA Magnetic Agarose Beads	Qiagen	Cat#36111
GFP-Trap beads	Chromotek	Cat#gta
SureBeads Protein G Magnetic Beads	Bio-Rad	Cat#1614023
TUBE1 magnetic beads	LifeSensors	Cat#UM401M
Control magnetic beads	LifeSensors	Cat#UM400M
Critical commercial assays		
Protein Fractionation Kit for Cultured Cells	Thermo Fisher Scientific	Cat#78840
PTMScan Ubiquitin Remnant Motif (K-ε-GG) Kit	Cell Signaling	Cat#5562
Lysosome Enrichment Kit for Tissues and Cultured Cells	Thermo Scientific	Cat#89839
Deposited data		
Mass spectrometry data for the ubiquitin-modified proteome analysis	PRIDE (Perez-Riverol et al., 2019)	PDX024211
Mass spectrometry data for lysosome enrichment	PRIDE (Perez-Riverol et al., 2019)	PDX024227
Mass spectrometry data for the LAMTOR1-GFP GlyGly-Site analysis	PRIDE (Perez-Riverol et al., 2019)	PDX024940
Mass spectrometry data for the LAMTOR1-GFP Interactome	PRIDE (Perez-Riverol et al., 2019)	PDX035974
Experimental models: Cell lines		
hTERT RPE1	ATCC	CRL-4000, RRID:CVCL_4388
U2OS	DSMZ	ACC 785, RRID:CVCL_0042
HEK293	DSMZ	ACC 305, RRID:CVCL_0045
HEK293T	DSMZ	ACC 635, RRID:CVCL_0063
MCF7	ATCC	HTB-22, RRID:CVCL_0031
Experimental models: Organisms/strains		
Bristol N2 wildtype	Caenorhabditis Genetics Center; (Brenner S., 1974)	N/A
adIs2122[lgg-1p::GFP-LGG-1; rol-6(su1006)]	Caenorhabditis Genetics Center; (Kang et al., 2007)	N/A

(*Continued on next page*)

Continued

REAGENT or RESOURCE	SOURCE	IDENTIFIER
sqIs17[hlh-30p::HLH-30-GFP; rol-6(su1006)]	Caenorhabditis Genetics Center; (Lapierre et al., 2013)	N/A
Oligonucleotides		
gRNA for CRISPR KO of USP32 1F (CACCGgaatgcacatgacaccacaa)	Sigma Aldrich	N/A
gRNA for CRISPR KO of USP32 1R (AAACttgtggtgtcatgtgcattcC)	Sigma Aldrich	N/A
gRNA for CRISPR KO of USP32 2F (AAACttgtggtgtcatgtgcattcC)	Sigma Aldrich	N/A
gRNA for CRISPR KO of USP32 2R (AAACggaaagaatgctccacgtggC)	Sigma Aldrich	N/A
gRNA for CRISPR KO of USP32 3F (CACCGcagttacgtgaatactacag)	Sigma Aldrich	N/A
gRNA for CRISPR KO of USP32 3R (AAACctgtagtattcacgtaactgC)	Sigma Aldrich	N/A
siPOOL USP32 (NCBI Gene ID: 84669	siTOOLs Biotech	N/A
siPOOL negative control	siTOOLs Biotech	N/A
Recombinant DNA		
pEGFPC1-GW-JJ-USP32	gift from Sylvie Urbé	N/A
pIRES-HA-USP32 (wt)	this study	N/A
pIRES-HA-USP32 (C743S)	this study	N/A
pAcGFP-C1-Rab7A	Addgene	Cat#61803
pcDNA-Myc3-Rab7A	this study	N/A
pcDNA-Myc3-Nrf2	Addgene	Cat#21555
pEGFP-N1-LAMTOR1	Addgene	Cat#42334
pEGFP-N1-LAMTOR1 K20R	this study	N/A
pRK5-LAMTOR1-HA	Addgene	Cat#42338
pEGFPN1	Clontech	Cat#6085-1
BSSK-8xHA-ubiquitin	gift from Stefan Müller	N/A
BSSK-8xHis-ubiquitin	gift from Stefan Müller	N/A
pLentiCRISPRv2	Addgene	Cat#52961
pPAX.2	Addgene	Cat#12260
pMD2.G	Addgene	Cat#12259
pGEX-6P3-RILP	Jimenez-Orgaz et al., 2018	N/A
Software and algorithms		
BioRender	BioRender	https://www.biorender.com
CellProfiler 3.1.9	Broad Institute (McQuin et al., 2018)	https://cellprofiler.org
Image Lab 5.2.1	Bio-Rad	https://www.bio-rad.com
ImageJ 1.52q	National Institute Health (Schneider et al., 2012)	https://imagej.nih.gov/ij/
MaxQuant 1.5.1, 1.6.14	Max-Planck-Institute of Biochemistry (Cox & Mann, 2008)	https://www.maxquant.org/
Perseus 1.6.7	Max-Planck-Institute of Biochemistry (Tyanova et al., 2016)	https://maxquant.net/perseus/
Prism 5.0b or 6	GraphPad Software	
FlowJo™ Software, Version 10.4.2	Becton, Dickinson and Company	https://www.flowjo.com
Snapgene 2.8.3	Insightful Science	https://www.snapgene.com/
Fiji (ImageJ)	National Institute of Health (Schindelin et al., 2012)	https://fiji.sc/

RESOURCE AVAILABILITY

Lead contact

Further information and requests for resources and reagents should be directed to and will be fulfilled by the lead contact, Anja Bremm (bremm@em.uni-frankfurt.de).

Materials availability

Plasmids and cell lines are available upon request to the lead contact. The authors declare no restrictions on the use of materials detailed herein.

Data and code availability

- The mass spectrometry data for the ubiquitin-modified proteome analysis have been deposited to the ProteomeXchange Consortium via the PRIDE[1] partner repository with the dataset identifier PRIDE: PXD024211.
- The mass spectrometry data for lysosome enrichment have been deposited to the ProteomeXchange Consortium via the PRIDE[1] partner repository with the dataset identifier PRIDE: PXD024227.
- The mass spectrometry data for the LAMTOR1-GFP GlyGly-Site analysis have been deposited to the ProteomeXchange Consortium via the PRIDE[1] partner repository with the dataset identifier PRIDE: PXD024940.
- The mass spectrometry data for the LAMTOR1-GFP Interactome analysis have been deposited to the ProteomeXchange Consortium via the PRIDE[1] partner repository with the dataset identifier PRIDE: PXD035974
- This paper does not report original code.
- Any additional information required to reanalyze the data reported in this paper is available from the lead contact upon request.

EXPERIMENTAL MODEL AND SUBJECT DETAILS

hTERT RPE1 cells were obtained from American Type Culture Collection (ATCC CRL-4000) and grown in DMEM/F-12, GlutaMAX™ medium (Gibco) supplemented with 10% (v/v) fetal bovine serum (Gibco), 200 μg/mL Hygromycin B, 50 U/ml penicillin and 50 μg/mL streptomycin (GE Healthcare) at 37°C and 5% CO_2. U2OS, HEK293, and HEK293T cells were obtained from Leibnitz Institute DSMZ-German Collection of Microorganisms and Cell Culture (DSMZ no. ACC 785, ACC 305, and ACC 635, respectively) and grown in DMEM, GlutaMAX™ medium (Gibco) supplemented with 10% (v/v) fetal bovine serum (Gibco) and 50 U/ml penicillin and 50 μg/mL streptomycin (GE Healthcare) at 37°C and 5% CO_2. MCF7 were obtained from American Type Culture Collection (ATCC HTB-22) and grown in DMEM, GlutaMAX medium (Gibco) supplemented with 10% (v/v) fetal bovine serum (Gibco), 50 U/ml penicillin and 50 μg/mL streptomycin, 1 mM sodium pyruvate and 0.1 mM non-essential amino acids. PCR-based Mycoplasma contamination tests were regularly performed using the Venor®GeM Classic kit (Minerva Biolabs).

C. elegans strains used in this study were cultivated on NGM (Nematode Growth Medium) agar plates at 20°C with OP50 E. coli as food source, if not otherwise stated.[58] The following strains have been used: wildtype Bristol N2, adIs2122[lgg-1p:GFP-LGG-1; rol-6(su1006)],[59] and sqIs17[hlh-30p:HLH-30-GFP; rol-6(su1006)].[60]

METHOD DETAILS

Cell transfection & treatment

For DNA transfection, cells were seeded to achieve 30-40% confluency the following day and transfected with PEI (polyethyleneimine, 25 kDa, linear, 1 mg/mL, Polysciences Europe). Transfection mix was prepared with a DNA:PEI ratio 1:3 for HEK293 cells and 1:5 for RPE1 cells in prewarmed Opti-MEM (Gibco/Life Technologies) and incubated for 10 min at room temperature before adding to cells. RPE1 cells were transfected in medium without supplements, medium was exchanged with full medium after 4 h. After transfection, cells were cultured for 18-24 h prior to lysis.

For siRNA transfection, 1 × 10^5 U2OS or RPE1 cells were seeded in a 6 well dish and reverse transfected with a final siRNA pool concentration of 3 nM using Lipofectamine RNAiMAX
(Invitrogen) following the siRNA manufacturer's reverse transfection protocol. The medium was exchanged after 24 h after transfection. Cells were cultured for additional 24 h prior to further treatment and lysis

Cell lysis and immunoblotting

Unless described differently for specific experimental procedures cells were lysed with RIPA buffer (50 mM Tris (pH 7.5), 150 mM NaCl, 1% (v/v) NP-40, 0.5% (v/v) Na deoxycholate, 0.1% (v/v) SDS, 1 × cOmplete, EDTA-free protease inhibitors (Roche), 1 × PhosSTOP phosphatase inhibitors (Roche), Benzonase) on ice for 10 min. Soluble fractions were isolated by centrifugation for 10 min at 13,000 rpm at 4°C. Cleared lysates were mixed with 4 × LDS sample buffer and boiled at 95°C for denaturation.

Proteins were separated by SDS-PAGE and transferred onto a PVDF membrane. After blocking for 1 h with 5% skim milk in TBS-T, blots were incubated overnight at 4°C with primary antibodies followed by incubation with secondary antibodies for 1 h in 5% skim milk in TBS-T at room temperature. Chemiluminescence signal was detected using the ChemiDoc Imaging System (Bio-Rad).

ImageJ[61] was used to measure band intensities of proteins of interest from Western blots. For relative quantification, the intensity values were normalized to the lane's loading control, and for phospho-proteins to the total protein, as well.

Antibodies

Following primary antibodies and their respective dilution for Western blotting or immunofluorescence were used:

Rabbit anti-ATP6V1A (ab199326, 1:2000), rabbit anti-Giantin (ab80864), rabbit anti-MPR (cation independent) (ab124767, 1:50.000), goat anti-VPS35 (ab10099, 1:1000), and mouse anti-WIPI2 (ab105459, 1:1000) were purchased from Abcam; mouse anti-CD222 (MCA2048) and sheep anti-TGN46 (AHP500G) were purchased from AbD Serotec, rabbit anti-VPS29 (Atlas Antibodies, HPA039748, 1:500); mouse anti-GM130 (BD Transduction Laboratories, 610822, 1:100); rabbit anti-ATP6V1B2 (14488, 1:1000) ,rabbit anti-Cathepsin D (2284, 1:500), rabbit anti-EGFR (2232, 1:1000), rabbit anti-Histone H2B (12364, 1:1000), rabbit anti-LAMTOR1 (8975, 1:1000, 1:100), rabbit anti-LC3 A/B (12741, 1:1500, 1:200), rabbit anti-mTOR (2983, 1:200), mouse anti-Myc-Tag (2276, 1:1500), rabbit anti-phospho-ULK1 (Ser757) (6888, 1:1000), rabbit anti-PARP (9542, 1:1000), rabbit anti-phospho-WIPI2 (Ser413) (13571, 1:1000), rabbit anti-Rab7 (9367, 1:1000), rabbit anti-Rab11 (5589, 1:2000), rabbit anti-TFEB (37785, 1:200), rabbit anti-α-Tubulin (2125, 1:1500), rabbit anti-Ubiquitin (3933, 1:1000), and rabbit anti-ULK1 (8054, 1:1000) were purchased from Cell Signaling Technology; mouse anti-LAMP1 (H4A3-c, 1:1000, 1:200) and mouse anti-LAMP2 (H4A4-c, 1:1000, 1:200) were purchased from the Developmental Studies Hybridoma Bank; mouse anti-GAPDH (60004-1-Ig, 1:2000) was purchased from Proteintech; mouse anti-Actin (A4700, 1:1000), rabbit anti-phospho-AMBRA1 (Ser52) (ABC80, 1:500), rabbit anti-USP32 (HPA044365, 1:1500, 1:200), mouse anti-Vinculin (V4505, 1:10000), mouse anti-VPS26A (AMAB90967, 1:500), and rabbit anti-VPS29 (HPA039748, 1:500) were purchased from Merck/Sigma-Aldrich; goat anti-Cathepsin X/Z/P (R&D Systems, AF934, 1:2000); mouse anti-AMBRA1 (sc-398204, 1:1000), mouse anti-GST (sc-138), and mouse anti-His-Tag (sc-53073, 1:1000) were purchased from Santa Cruz Biotechnology

Following secondary antibodies and their respective dilutions were used:

horse anti-mouse IgG-HRP (7076, 1:5000), and goat anti-rabbit IgG-HRP (7074, 1:5000) were purchased from Cell Signaling Technology; donkey anti-goat IgG-HRP (sc-2020, 1:10000), donkey anti-mouse IgG-HRP (sc-2096, 1:10000), and goat anti-rabbit IgG-HRP (sc-2054, 1:10000) were purchased from Santa Cruz Biotechnology; goat anti-mouse IgG Alexa Fluor 647 (A-21235, 1:200), donkey anti-rabbit IgG Alexa Fluor 488 (A-21206, 1:200), and donkey anti-rabbit Alexa Fluor 647 (A-31573, 1:200) were purchased from Thermo Fisher Scientific

Immunofluorescence staining and confocal microscopy

For immunofluorescence microscopy, cells were grown on uncoated glass coverslips in 6 well plates (Greiner). After treatment as indicated, cells were fixed with cold 4% paraformaldehyde (PFA) solution in phosphate buffered saline (PBS, Santa Cruz) for 15 min, washed twice with PBS and permeabilized with 1% Triton X-100 (Carl Roth) in PBS for 15 min followed by a final wash with PBS. For LC3 staining, cells were fixed and permeabilized with ice-cold methanol for 15 min at −20°C. Samples were blocked with 2.5% BSA (BSA, Carl Roth) in PBS with 0.05% Tween 20 (Sigma Aldrich) (BSA-PBS-T) for 30 min. Primary antibodies were applied as indicated in the described dilution in BSA-PBS-T for 1 h at room temperature (RT). Afterward samples were washed three times for 5 min with PBS to remove residual antibody and incubated with corresponding fluorescently labeled secondary antibody in 1:200 dilution in BSA-PBS-T for 1 h at RT. After additional washing with PBS (three time for 5 min) cells were mounted using ProLong Diamond Antifade Reagent mounting medium with DAPI (Life Technologies).

Images were acquired on either a confocal Zeiss LSM780 or Leica SP8 LSM with a 40x or 63× oil-immersion objective in 512× 512 or 1024 × 1024 scanning format using the standard Zeiss Zen or Leica LaX software. For each image, color channels were saved separately in TIF file format for post-collection processing. Quantification was performed with the open-source cell image analysis software CellProfiler (version 3.1.9).[62]

Results from repeat experiments were analyzed for statistical significance by a two-tailed, unpaired Student's *t* test between the indicated conditions using GraphPad Prism (version 5.0b for Mac, GraphPad Software, San Diego, California USA, www.graphpad.com).

Brightness and contrast were increased for all channels and conditions uniformly across the entire image using ImageJ[61] where necessary for better visibility in the final figure.

Flow cytometry

U2OS cells stably expressing pMRX-IP-GFP-LC3-RFP-LC3ΔG (gift from Noboru Mizushima, Addgene plasmid #84572) were grown in 6-well plates. After the indicated treatment, cells were washed with PBS, trypsinized in 100 μL 0.05% Trypsin-EDTA, and collected in 500 μL PBS. Cells were passed through a cell strainer cap into the FACS test tubes (Falcon) and kept on ice until measurement on a SH800S Cell Sorter (SONY). Data were analyzed and figures were created using FlowJo (Version 10.4.2, FlowJo, LLC).

Subcellular fractionation

Subcellular fractionation of RPE1, U2OS and MCF7 cells was performed using the Subcellular Protein Fractionation Kit for Cultured Cells (78,840, Thermo Fisher Scientific) according to manufacturer's protocol.

CI-MPR uptake assays

The parental and USP32 KO cells were seeded onto glass coverslips and grown to 50-70% confluency in 12-well plates. Cells were then incubated with a mouse monoclonal antibody against the extracellular domain of the CI-MPR (mouse anti-CD222, AbD Serotec) at 10 μg/mL in full growth DMEM for the indicated periods at 37°C, followed by washing in cold PBS and fixation in ice-cold 4% PFA in PBS. Cells were then permeabilized with 0.1% Saponin, blocked with 1% BSA in PBS for 30 min and stained with an antibody against TGN46 (sheep anti-TGN46, AbD Serotec) and also with an anti-mouse secondary antibody to visualize the internalized antibody. The colocalization between the internalized anti-CI-MPR antibody and TGN46 was then analyzed using the colocalization tool of the Volocity 6.1 software package (PerkinElmer) after setting of uniform thresholds across conditions. The quantification of the colocalization was performed over ten images (each) from two independent experiments, followed by testing of significance with an unpaired t test.

RILP assay

Full length GST-RILP protein was expressed in BL21(DE3) bacteria using pGEX-6P3 (GE Healthcare) with standard procedures and purified using GSH-Sepharose (GE Healthcare). Parental and USP32 KO RPE1 cells grown in 6 cm dishes were lysed in 0.5 mL lysis buffer (Tris-HCL, pH 7.8, 50 mM NaCl, 0.5% Triton X-100, 1 mM $MgCl_2$ and Roche protease inhibitor without EDTA). 10% of the lysate was kept for the respective Input analysis. GST-control beads and GST-RILP beads were then incubated with the respective lysates for 2 h at 4°C, followed by two washing steps in lysis buffer and Western blot based detection of bound Rab7 and total Rab7 from the retained Input lysates.

His-Ubiquitin pulldown

Ubiquitination of Myc-Rab7 or LAMTOR1-GFP was assessed by co-expression with wildtype or catalytic dead HA-USP32 together with His- or HA-tagged (for control) ubiquitin in HEK293 cells. 48 h after transfection, cells were lysed for 15 min at 99°C with lysis buffer (6 M Guanidin-HCl, 0.1M NaH_2PO_4, 0.05% Tween 20, 0.1 M Tris, pH 8). Lysates were cleared by high-speed centrifugation at 13,000 rpm for 10 min 10% of lysate was removed for input sample and prepared for immunoblotting by TCA precipitation. Ni-NTA Magnetic Agarose Beads (3611, Qiagen) were washed twice with lysis buffer and added to the cleared lysates. Pulldown was incubated overnight at RT while rotating. Beads were washed three times with wash buffer A (8 M Urea, 0.1 M NaH_2PO_4, 0.05% Tween 20, 0.01 M Tris, pH 8), then washed twice with wash buffer B (8 M Urea, 0.1 M NaH_2PO_4, 0.05% Tween 20, 0.01 M Tris, pH 6.4). Last washing step was performed using PBS. Beads were resuspended in 2 × LDS sample buffer containing 20 mM DTT. Samples were boiled for 10 min at 95°C and subjected to immunoblotting.

TUBE PD

Ubiquitinated proteins were enriched by using Tandem Ubiquitin Binding Entities (TUBEs). RPE1 cells were lysed for 20 min at 4°C with lysis buffer (50 mM Tris, 150 mM NaCl, 1 mM EDTA, 1% NP-40, 10% Glycerol, including PhosStop phosphatase inhibitors, cOmplete protease inhibitors and 20 mM NEM). Lysates were cleared by highspeed centrifugation at 13,000 rpm for 10 min at 4°C and transferred to a fresh tube. 5% of lysate was removed for the input sample and prepared for immunoblotting. 40 μL TUBE1 magnetic beads (LifeSensors) or Control magnetic beads (LifeSensors) were washed twice with 1 mL wash buffer (20 mM Tris, 150 mM NaCl, 0.1% Tween 20) and added to the lysates. Pulldown was incubated rotating overnight at 4°C. The next day, beads were magnetized and the supernatant was removed. The samples were washed three times with 500 μL cold wash buffer and afterward resuspended in 40 μL 2xLDS sample buffer containing 20 mM DTT. Samples were boiled for 10 min at 95°C and subjected to immunoblotting.

LAMTOR1-GFP immunoprecipitation

LAMTOR1-GFP was immunoprecipitated from transfected RPE1 cells using GFP-Trap Agarose beads (gta, ChromoTek). 24 h after transfection, cells were lysed for 20 min at 4°C with lysis buffer (20 mM Tris pH 7.5, 150 mM NaCl, 0.5% Triton X-100, including PhosStop phosphatase inhibitors (4,906,837,001, Merck/Roche), cOmplete protease inhibitors (4693132001, Merck/Roche) and 20 mM NEM). Lysates were cleared by high-speed centrifugation at 13000 rpm for 10 min at 4°C. GFP-Trap beads were washed twice with wash buffer (20 mM Tris pH 7.5, 150 mM NaCl) and added to the lysates. Samples were incubated rotating for 1-2 h at 4°C. Beads were washed three times with wash buffer and prepared either for immunoblotting or mass spectrometry analysis.

Interactome and GlyGly-Site analysis

After the final IP wash, samples were washed additionally three times with wash buffer. Elution buffer (2% Na-deoxycholate, 1 mM TCEP, 4 mM Chloroacetamide (CAA), 50 mM Tris pH 8.5) was added directly to beads and samples were boiled for 10 min at 60°C. The cooled down samples were incubated with 500 ng LysC/Trypsin in 50 mM Tris pH 8.5 over night at 37°C. Digested samples were

mixed with isopropanol and TFA to stop the digestion and directly loaded on in-house assembled SDB-RPS STAGE tips. Following two wash steps with 1% TFA in isopropanol and 0.2% TFA in water, peptides were eluted with 1.25% ammoniumhydroxide in 80% ACN and dried for storage.

Dried peptides were reconstituted in 2% ACN, 0.1% TFA and analyzed on a Q Exactive HF mass spectrometer coupled to an easy nLC 1200 (ThermoFisher Scientific) using a 35 cm long, 75 μm ID fused-silica column packed in house with 1.9 μm C_{18} particles (Reprosil pur, Dr. Maisch), and kept at 50°C using an integrated column oven (Sonation). Peptides were eluted by a non-linear gradient from 4-28% acetonitrile over 45 min and directly sprayed into the mass-spectrometer equipped with a nanoFlex ion source (ThermoFisher Scientific). Full scan MS spectra (300-1650 m/z) were acquired in profile mode at a resolution of 60,000 at m/z 200, a maximum injection time of 20 ms and an AGC target value of 3×10^6 charges. Up to 15 most intense peptides per full scan were isolated using a 1.4 Th window and fragmented using higher energy collisional dissociation (normalised collision energy of 28). MS/MS spectra were acquired in centroid mode with a resolution of 30,000, a maximum injection time of 45 ms and an AGC target value of $1 \times 10.^5$ Single charged ions, ions with a charge state above 6 and ions with unassigned charge states were not considered for fragmentation and dynamic exclusion was set to 20 s to minimize the acquisition of fragment spectra of already acquired precursors.

MS raw data was processed with MaxQuant (v 1.6.14.0 for GlyGly-Site analysis, v 1.6.17.0 for Interactome analysis) applying default parameters. Acquired spectra were searched against the human "one sequence per gene" database (Taxonomy ID 9606) downloaded from UniProt (2020-03-12; 20531 sequences for GlyGly-Sites, 2022-04-17, 20509 sequences for Interactome), and a collection of 244 common contaminants ("contaminants.fasta" provided with MaxQuant) using the Andromeda search engine integrated in MaxQuant.[63,64] Searches were performed using default parameters but adding the GlyGly-remnant on Lysines as a variable modification. Identifications were filtered to obtain false discovery rates (FDR) below 1% for GlyGly-sites, peptide spectrum matches (PSM; minimum length of 7 amino acids) and proteins using a target-decoy strategy.[65] Protein quantification and data normalization relied on the MaxLFQ algorithm implemented in MaxQuant.[66]

The MaxQuant output ("proteinGroups.txt", "GlyGly(K)sites.txt") was processed in Perseus (v. 1.6.7.0,.[67] First, proteins only identified by a single modified peptide ("only identified by site") or matching to the reversed or contaminants databases were removed. For interactome analysis, iBAQ intensities were used and only proteins with at least two valid values in the respective IP-sample were kept for statistical analysis following the imputation of missing values in the Control-group (GFP-only) by drawing random numbers from a normal distribution (width: 0.3, down-shift: 1.8). Interactors were defined by a right-sided Student's t test against the Control-group, applying a p value ($p < 0.05$) and a fold-change ($FC > 2$) filter. The resulting iBAQ-values of bona fide interactors (282 proteins) were normalized with CyclicLoess and differentially interacting proteins defined using limma, both using the NormalyzerDE package in R (v. 3.6.3) via R Studio (v. 2022.02.0, "Prairie Trillium").

For the analysis of the GlyGly-sites, only sites quantified in at least 2 replicates in each condition (NHT, USP32 KO) were considered and missing values were not imputed. Significantly changing GlyGly-sites were defined by a Student's t test (p value <0.05) adding an additional minimum fold-change cut-off (>1.5).

Co-immunoprecipitation

Endogenous VPS35 was co-immunoprecipitated from RPE1 cells. Cells were lysed for 20 min at 4°C with lysis buffer (20 mM Tris pH 7.5, 150 mM NaCl, 0.5% Triton X-100, including PhosStop phosphatase inhibitors (4906837001, Merck/Roche) and cOmplete protease inhibitors (4693132001, Merck/Roche)). Lysates were cleared by high-speed centrifugation at 13,000 rpm for 10 min at 4°C. 10% of lysate were removed for the input sample and prepared for immunoblotting. SureBeads™ Protein G Magnetic Beads (1614023, Bio-Rad) were washed three times with lysis buffer. A pre-clearing step of the lysates was performed with unloaded beads rotating for 1 h at 4°C. Beads for pre-clearing were discarded. IgG control or VPS35 antibody was added to the pre-cleared lysates. Samples were incubated rotating at 4°C for 1 h. Washed SureBeads were added and IP was incubated additionally for 1 h at 4°C. Beads were washed three times with lysis buffer. Samples were eluted with 2 × LDS sample buffer for 10 min at 95°C. Afterward 50 mM DTT was added and boiled again for protein denaturation. Samples were subjected to immunoblotting.

Ubiquitin-modified proteome analysis (diGly remnant profiling)

RPE1 cells were grown for two weeks in DMEM suitable for SILAC labeling containing either light (K0R0) or heavy (K8R10) lysine and arginine. Cells were lysed for 15 min on ice with modified RIPA lysis buffer (50 mM Tris pH 7.5, 150 μM NaCl, 1 mM EDTA, 1% NP-40, 0.1% Na-deoxycholate, including PhosStop phosphatase inhibitors (4906837001, Merck/Roche), cOmplete protease inhibitors (4693132001, Merck/Roche) and 20 mM NEM). Lysates were sonicated and cleared by centrifugation for 15 min at 13,000 rpm at 4°C. Protein concentration was measured using Bradford assay and lysates from heavy and light labeled samples were combined in a 1:1 ratio. (50 μg protein of sample were used for later full proteome analysis.) Proteins were precipitated in 80% ice-cold acetone at −20°C overnight. Washed and dried pellets were dissolved in denaturation buffer (6 M urea, 2 M thiourea, 10 μM HEPES pH 8.0) and subjected to in-solution digest. Proteins were reduced with 1 mM DTT, alkylated with 5 mM CAA and digested with 1 μg/μL LysC/200 μg protein for 4 h and subsequently with 1 μg/200 μg protein Trypsin overnight. Digest was stopped with 0.5% TFA. Peptides were purified on C_{18} SepPak columns and eluted with 50% ACN.

The immunoaffinity purification (IAP) for ubiquitinated peptides was performed using the PTMScan Ubiquitin Remnant Motif (K-ε-GG) Kit (5562, Cell Signaling). Purified peptides were concentrated in 10x IAP buffer. PTMScan Ubiquitin Remnant Motif

(K- ε -GG) Antibody beads were washed three times with IAP buffer, peptides were added and incubated rotating for 4 h at 4°C. Beads were washed two times with IAP buffer containing 150 mM NaCl and 0.5% NP-40, two times with IAP buffer only and two times with water. Peptides were eluted from beads in a four step procedure using 0.15% TFA. IAP eluents were fractionated using SCX STAGE tips. After loading the peptides onto SCX STAGE tips, samples were washed with 0.1% TFA in 40% ACN and eluted with increasing pH of elution buffer (24 mM acetic acid (AA), 24 mM boric acid, 24 mM phosphoric acid in 40% ACN).

For the full proteome analysis, 50 μg protein sample were mixed with LDS and 10 mM DTT and boiled for 10 min at 70°C. 55 mM CAA was added and samples were separated on a 10% SDS-PAGE followed by Coomassie protein staining with InstantBlue (Expedeon). Gel lanes were cut into equal pieces and subjected to in-gel digestion. Gel pieces were destained with 40% EtOH in 50 mM ammonium bicarbonate (ABC) and dehydrated in 100% EtOH. Proteins were reduced with 10 mM DTT, alkylated with 55 mM CAA and digested with 5 ng/μL Trypsin overnight. Elution of peptides was performed using an increasing acetonitrile (ACN) concentration from 30% to 100%.

Purification and concentration for proteome and IAP samples was performed using C_{18} STAGE tips. Peptides in 1% TFA in 2% ACN were loaded on in-house assembled C_{18} STAGE tips and washed with 0.5% AA. Elution was performed with 80% ACN in 0.5% AA and peptides were dried afterward. For LC-MS analysis, peptides were rehydrated in 0.1% TFA and 2% ACN. Purification and concentration for proteome and IAP samples was performed using C_{18} STAGE tips. Peptides in 1% TFA in 2% ACN were loaded on in-house assembled C_{18} STAGE tips and washed with 0.5% AA. Elution was performed with 80% ACN in 0.5% AA and peptides were dried afterward. For LC-MS analysis, peptides were rehydrated in 0.1% TFA and 2% ACN.

Peptides were loaded with an easy nLC1200 onto a self-made 15 cm column filled with 1.7μm C18 particles. For the analysis of peptides obtained by diGly enrichment, the peptides were separated with a 58 min gradient from 10 to 38% B (B being 0.1% formic acid in 95% acetonitrile and A being 0.1% formic acid in acetonitrile in water.). The eluting peptides were directly injected into an Q Exactive HF operating in DDA mode. In brief after a survey scan 60,000 resolution the 10 most abundant precursor ions were fragmented by HCD and the resulting fragments analyzed with 30,000 resolution. Only precursors with charge states 3-7 were taken into account for fragmentation and afterward dynamically excluded for 20 s. After the gradient, the column was washed with 100% B and reequilibrated for a total analysis time of 75 min. For analysis of peptides prepared by the gel-based approach, the analysis was the same, but the number of precursor ions chosen for fragmentation (15) and that also precursor ions with a charge of 2 were subjected to further analysis.

Data analysis was done with MaxQuant 1.5.1 against the Uniprot Human Reference Proteome database with standard settings and activated SILAC quantification (K8). For analysis of the samples from the diGly approach diGly modification of Lysines were set as an additional variable modification. Ratios for peptides with diGly modification were adjusted to total protein level by correction with the data from the total protein experiment. Differentially abundant peptides harboring a diGly motif ($p < 0.01$) were detected with a Student's *t* Test with Perseus.

Lysosome enrichment

Enrichment of lysosomal fraction from U2OS or RPE1 cells was performed by density gradient centrifugation using the Lysosome Enrichment Kit for Tissues and Cultured Cells (89839, Thermo Fisher Scientific) according to manufacturer's protocol. Samples were prepared for immunoblotting.

Lysosome proteome

U2OS cells were grown for two weeks in DMEM suitable for SILAC labeling containing either light (K0R0) or heavy (K8R10) lysine and arginine. Lysosome fraction was enriched as described above. Proteins were separated on a 10 % SDS-PAGE followed by Coomassie protein staining with InstantBlue (Expedeon). Gel lanes were cut into equal pieces and subjected to in-gel digestion. Gel pieces were destained with 40% EtOH in 50 mM ammonium bicarbonate (ABC) and dehydrated in 100 % EtOH. Proteins were reduced with 10 mM DTT, alkylated with 55 mM CAA and digested with 5 ng/μL Trypsin overnight. Elution of peptides was performed using an increasing acetonitrile (ACN) concentration from 30% to 100%. Peptides in 1% TFA in 5% ACN were loaded on in-house assembled C_{18} STAGE tips and washed with 0.5% acetic acid (AA). Elution was performed with 80% ACN in 0.5% AA and peptides were dried afterward. For LC-MS analysis, peptides were rehydrated in 0.1% TFA and 2% ACN.

The LC-MS analysis was performed as described above for the proteome samples, but with a shorter gradient of 23 min for a total run time of 35 min.

Data analysis was done with MaxQuant 1.5.1 against the Uniprot Human Reference Proteome database with standard settings and activated SILAC quantification (K8, R10). Differentially abundant proteins ($p < 0.05$) were detected with a Student's *t* Test with Perseus.

Guide RNA design and CRISPR/Cas9 plasmid generation

USP32 knockout RPE1 cells were generated using the CRISPR/Cas9 technology. Guide RNA sequences targeting spCas9 to the genomic locus of USP32 (ID Ensembl ENSG00000170832) were designed according to.[68] Specific overhangs for subsequent ligation into pLentiCRISPRv2 (gift from Feng Zhang, Addgene plasmid #52961) were added to each guide (underlined):

USP32_KO-1-F: CACCGgaatgcacatgacaccacaa USP32_KO-1-R: AAACttgtggtgtcatgtgcattcC

USP32_KO-2-F: CACCGccacgtggagcattctttcc USP32_KO-2-R: AAACggaaagaatgctccacgtggC
USP32_KO-3-F: CACCGcagttacgtgaatactacag USP32_KO-3-R: AAACctgtagtattcacgtaactgC

Complementary oligonucleotides were annealed for 5 min at 95°C, and subsequently cooled down for 15 min at room temperature. Annealed primers were diluted to 0.5 μM in nuclease free water and cloned into pLentiCRISPRv2 via *Bsm*BI restriction enzyme (NEB) digest and subsequent ligation with T4 DNA ligase (NEB). Stellar competent cells (Clontech) were transformed with the ligation reaction and correct clones were identified by SANGER sequencing (Microsynth SeqLab) using the U6 primer.

Generation of high titer lentivirus and viral transduction

7.5×10^5 HEK293T cells were seeded into a six-well plate and cultivated in DMEM medium without antibiotics 24 h prior to transfection. Cells were transfected with Lipofectamine 2000 (Invitrogen/Life Technologies) by mixing the reagent with 200 μL Opti-MEM and 3.3 μg transfer vector containing the gRNAs (pLentiCRISPRv2), 2.7 μg PAX2 (a gift from Didier Trono, Addgene plasmid #12260) and 1 μg pMD2.G (a gift from Didier Trono, Addgene plasmid #12259). The transfection mix was incubated for 30 min at room temperature and afterward dropwise added to HEK293T cells. Medium was replaced with fresh DMEM containing 10% (v/v) fetal bovine serum (Gibco/Life Technologies) and 50 U/ml penicillin and 50 μg/mL streptomycin (GE Healthcare) 12 h after transfection. Supernatant containing lentiviral particles was collected after 24 h and 48 h. Supernatants were pooled and frozen at −80°C.

For viral transduction, supernatants were thawed at room temperature, sterile filtered through 0.45 μm filters and mixed with 10 μg Polybrene (Sigma-Aldrich) to infect 1×10^6 RPE1 cells. Stable transduced cells were selected with puromycin and efficiency of USP32 knockout was confirmed by immunoblotting.

DNA and siRNA constructs

All cloning was done using the In-Fusion cloning system (In-Fusion HD Cloning Kit, Clontech) according to manufacturer's instructions. Oligonucleotide primers were designed with the Snapgene software's build-in In-Fusion Cloning tool (Insightful Science; available at snapgene.com) and purchased from Sigma-Aldrich.

Mammalian expression vector pEGFPC1-GW-JJ-USP32 (gift from Sylvie Urbé) was used as template for cloning USP32 into pIRES-HA-C1 vector using the *Not*I restriction site.

pcDNA-Myc3-Rab7A was generated using pAcGFP-C1-Rab7A (gift from Gia Voeltz, Addgene plasmid #61803) as template to amplify Rab7A. The insert was cloned into pcDNA-Myc3-Nrf2 (gift from Yue Xiong, Addgene plasmid #21555) by exchanging the Nrf2 gene using the *Bam*HI and *Xba*I restriction sites.

pEGFP-N1-LAMTOR1 was a gift from David Sabatini (Addgene plasmid #42334). BSSK-8×His-Ubiquitin and BSSK-8×HA-ubiquitin were gifts from Stefan Müller.

Site directed mutagenesis was performed using the QuickChange Method. Mutagenesis primers for USP32 (C743S) and LAMTOR1 (K20R) were generated with the QuickChange Primer Design Tool (Agilent). pIRES-HA-USP32 or pEGFPN1-LAMTOR1 were used as template and PCR was performed using Phusion High-Fidelity DNA Polymerase (NEB, M0530S) according to manufacturer's protocol.

siRNA oligonucleotide pools were purchased from siTOOLs Biotech: siPOOL USP32 (NCBI Gene ID: 84,669) and negative control siPOOL.

C. elegans RNA interference and drug treatment

RNAi knockdowns experiments were applied by feeding worms HT115(DE3) bacteria transformed with a vector to express double-strand RNA (dsRNA) for a specific gene of interest after IPTG induction from a T7 promoter based system according to the standard protocol.[69] NGM RNAi plates contained 1 mM IPTG and 50 μg/mL Ampicillin, if not otherwise stated. To allow the embryonic development to proceed undisturbed worms were exposed to the double dsRNA from hatching to adulthood. The RNAi phenotypes were scored in one-day adult animals. The cDNAs of the genes of interest were cloned into the standard RNAi vector L4440 by restriction cloning, confirmed by sequencing and transformed into HT115(DE3) bacteria. For cyk-3 RNAi, two RNAi clones were constructed either containing the 5′ part of the cDNA (clone1) or the 3′ part (clone2). As control RNAi the empty vector L4440 was used. For metformin treatment, worm culture RNAi plates were prepared containing 50mM metformin (Sigma-Aldrich) as described in.[40]

C. elegans live-cell imaging microscopy

Mounting of adult worms has recently been described elsewhere.[70] We performed microscopy with a VisiScope spinning disk confocal microscope system (Visitron Systems, Puchheim, Germany) based on a Leica DMi8 inverted microscope, a Yokogawa CSU X1 scan head, a Hamamatsu ORCA-Flash 4.0 CC1140 and a SuperResolution upgrade extension GATACA LiveSR system. We performed all acquisitions at 21-23°C, using a Leica HC PL APO 63x/1.4-0.6 oil objective.

QUANTIFICATION AND STATISTICAL ANALYSIS

All statistical tests for experimental data obtained from human cells were performed using GraphPad Prism6; p values less than 0.05 were considered to be significant. Data were analyzed by *t* test, n numbers are indicated in figure legends.

For *C. elegans*, we performed threshold and intensity density measurements on Fiji (ImageJ).[71] When two samples were compared, a two-sided Student's *t* test was employed. For multiple samples comparison, a one-way ANOVA followed by a Bonferroni post-hoc test were used with GraphPad Prism6. Statistical details can be found in the figure legends for each experiment. The level of significance is shown in asterisks as follows: ***p < 0.001, **p < 0.01, *p < 0.05, not significant (n.s.) p > 0.05.